Quest Journals
Journal of Research in Environmental and Earth Sciences
Volume 9 ~ Issue 4 (2023) pp: 08-36
ISSN(Online) :2348-2532
www.questjournals.org

Research Paper

Modeling and simulation studies for leaching of some valuable metals from Southwestern Sinai, Egypt

Walaa A. Kassab, Ebrahim A. Gawad, Shimaa Salah, Amany R. Salem
Nuclear Materials Authority, Cairo, Egypt
P.O. Box 530 El Maadi, Cairo, Egypt
*The corresponding author: Walaa A. Kassab***:** *walaakassab22@gmail*

Abstract
Hydrometallurgy leaching is a common method for recycling valuable and heavy metals from their primary/or secondary resources. Herein, Gibbsite ore material contains REEs and valuable metal ions (e.g., Zn and Ni). The integrated Gibbsite perspective treatments for recovering the precious metals from the obtained optimal financial and technological was studied. The leaching processes were performed in a batch system. The effects of different leaching agents (sulfuric acid and ammonium sulfate) for extracting valuable elements from the working ore were compared and evaluated in detail. The optimum leaching conditions achieved by acidic leaching are 200 g/L H_2SO_4 acid within 4 h agitation time, 400 rpm agitation speed at 353 K, and a liquid/solid (L/S) ratio of 4/1. Under these conditions, the leaching efficiency of REEs, Zn, and Ni was about 91.88 %, 89.21 %, and 85.25 %, respectively. Different mathematical models represented that the leaching kinetics were investigated. The apparent activation energy was evaluated. Several new models were also simulated, and their validation of the leaching process was applied. The leaching procedure was used to simulate a number of novel models and apply their validations. A suggested floatotherm integrating the Vant-Hoff parametric model demonstrated endothermic and spontaneous behavior with increased randomness at the solid/solution contact during the acidic digestion of the Gibbsite ore materials.

Keywords: *REEs, Zn, Ni; Dissolution; Kinetic; Activation energy; Thermodynamics*.

Received 18 Mar., 2023; Revised 01 Apr., 2023; Accepted 03 Apr., 2023 © The author(s) 2023. Published with open access at www.questjournals.org

I. Introduction

Talet Seleim area is situated in southwestern Sinai, Egypt, between 33°20' and 33°25' E longitudes and 29°00' to 29°05' N latitudes Figure (1). It is covered mainly by the early Carboniferous Um Bogma Formation. The presence of a variety of metal values, such as U, Zn, REEs, Mn, Al, Co, Ni, and Cu, distinguishes this study rock sample [1-3]. The main minerals associated with gibbsite horizons in Abu Zeneima area are gibbsite, gypsum, halite, calcite, allanite, quartz, dolomite, and Mn oxides as well as berryite, goethite, and Cu minerals [4].

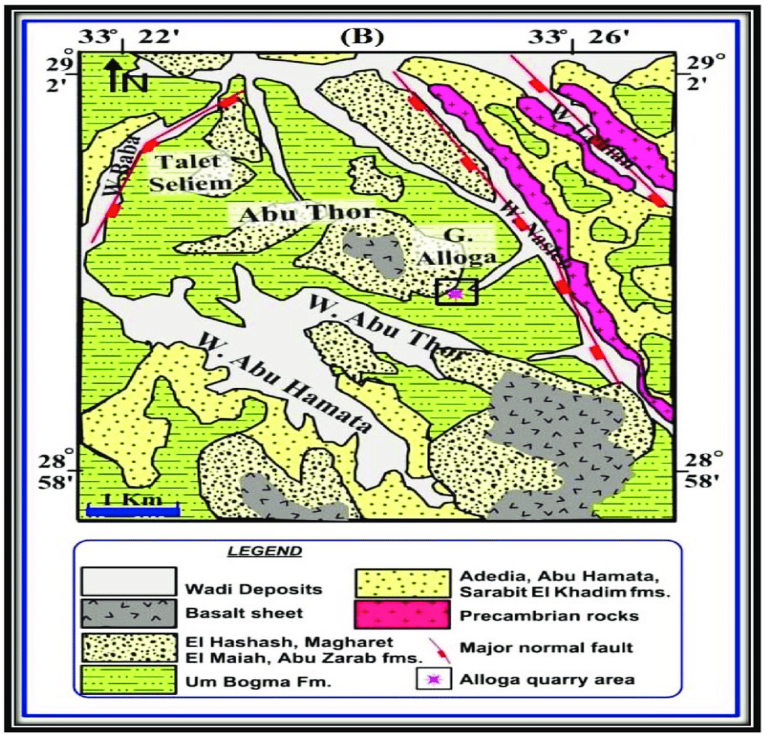

Figure (1): Geologic map of southwestern Sinai area (including Talet Seleim).

There is an increasing demand for the recovery of nickel (Ni), zinc (Zn), and REEs economic elements in the industry from mining tailings or tailings. Nickel is a valuable base metal with a wide range of applications [5]. Nickel can be found in batteries, corrosion-resistant alloys, stainless steel, electroplating, fuel cells, medical applications, nuclear power plants, and other applications [6-9].

Nickel can be found in sulfide ores, laterite ores, secondary resources, and non-land resources such as sea nodules [10,11]. Lateritic ores and sulfides are the main important sources of nickel [10,12-15]. Brazil has the third largest reserve and, according to the U.S. Geological Survey [9,15], the sixth largest nickel producer in the world. Pentlandite [$(Ni, Fe)_9S_8$] and nickel-bearing pyrrhotite are the two major Ni minerals in sulfide ores.

There are various techniques that can be used in the extraction of nickel from various ore minerals [16]. Nickel can be extracted from laterite ores [17] using both pyrometallurgical and hydrometallurgical processes. But the choice mainly depends on the mineralogical composition and the energy costs for processing the ore [9,18].

Ni extraction from laterite ores can be performed with acid leaching, which is one of the hydrometallurgical methods which includes high-pressure acid leaching (HPAL), heap leaching (HL), and atmospheric acid leaching (AL) [19-22] [23,24]. HPAL is one of the most commonly used processes for leaching low-grade laterite ores on an industrial scale [9]. Many hydrometallurgical studies have been made to develop new methods of exploiting laterite resources, including ammonia, hydrochloric acid, sulfuric acid, and biotechnologies [25,26,7]. The sulfuric acid pressure leach (PAL) process has been preferred to extract nickel and cobalt from laterites. The atmospheric hydrometallurgical hydrochloric acid-based leaching process for treating nickel-bearing laterites of various types has been described [27]. Therefore, developing a more economical and environmentally friendly process is of the utmost interest and importance in scientific research in laterite metallurgy.

Zinc is one of the most commonly consumed metals, ranking fourth after aluminum, iron, and copper [28]. Nowadays, Zn is mainly produced by hydrometallurgical processes, including roasting, leaching, cleaning, and electrowinning [29]. The main purpose of roasting is to convert ZnS into ZnO and $ZnSO_4$, which is beneficial for the subsequent leaching process [30]. However, roasting also has various disadvantages, such as high energy consumption and environmental pollution. Compared with the traditional technological ways, acid leaching with oxygen pressure is more attractive due to high metal yield and shortening of leaching time [31,32]. Therefore, in some scientific studies, a hydrometallurgical process based on the pressurized oxidative acid leaching of zinc sulfide concentrates has been applied for the direct production of zinc sulfate solution [33].

Lanthanides are a group of 15 chemically similar metals from La to Lu that, together with yttrium (Y) and scandium (Sc), form the group of rare earth elements (REEs). Their unique properties make them a material

of choice for various applications, and their requirements have been increasing in recent years [34,35]. Indeed, REEs are essential for designing new technologies such as wind turbines, hybrid cars, and mobile phone speakers [36]. Rare earth elements (REEs) have been used in green technology applications, such as neodymium (Nd), praseodymium (Pr), and dysprosium (Dy) for permanent magnets in wind turbines and lanthanum (La) and cerium (Ce) for batteries in electric vehicles due to their unique physicochemical properties [36].

Nowadays, the increasing use of wind energy and electric vehicles leads to high demand for REEs. Hydrometallurgy is preferable to pyrometallurgy for metal recycling in spent NiMH batteries due to its high yield, low energy requirements, and low greenhouse gas (GHG) emissions [37,38]. However, leaching valuable metals from spent NiMH batteries requires concentrated mineral acids and is also time-consuming [38,10]. Using spent acid to leach metals from e-waste would be environmentally friendly through waste recycling, knowing that significant amounts of phosphoric acid (H_3PO_4), sulfuric acid (H_2SO_4), hydrochloric acid (HCl), nitric acid (HNO_3), and hydrofluoric acid (HF) are used in cleaning processes in semiconductor production [39]. Meanwhile, the separation and purification of REEs from mixed leach solutions is a challenging topic that has been studied by liquid-liquid extraction [40], ion exchange [41], and ionic liquid [42,43]. Direct precipitation to recover REEs from the leach solution is an alternative by choosing an appropriate precipitating reagent and pH [44].

The main objective of the present study is to (1) leaching of REEs, Ni, and Zn from the study ore material by using sulfuric acid, (2) optimization of the leaching factors like leaching agent concentration, solid/liquid ratio, leaching time, and temperature, (3) study the influence of pH value on the leaching process, (4) Then performing kinetics, reaction mechanism, a kinetic model, activation energy and thermodynamic studies for the leaching process.

II. Experimental Procedure

2.1. Materials

All chemicals and reagents used in all different parts of this work are of analytical grade. The provided ore sample was collected from Gibbsite Ore materials of a Talet Seleim area. It was crushed by a laboratory jaw-crusher followed by grinding to 200 µm particle size. The ore was then quartered to have a representative sample for the chemical analyses.

2.2. Analytical methods

The control analysis of REEs was spectrophotometrically determined using the chromogenic reagent, Arsenazo-III [47], while for the determination of Zn and Ni, an atomic absorption spectrometer (Unicam 969, England) was used [45,46]. Major oxides SiO_2, TiO_2, Al_2O_3, and P_2O_5 were analyzed spectrophotometrically using a UV-Visible double-beam spectrophotometer (Shimadzu model (UV-11601) from Japan) [47]. The spectrophotometer ranges from 190 to 1100 nm, with a resolution of 2 nm and a wavelength accuracy of 0.5 nm. The Sherwood 410 flame photometer was used to photometrically determine the Na and K content, while total Fe was reported as Fe_2O_3, MgO, and CaO were determined volumetrically by titration methods [47]. To ensure reproducibility, the experiments/analysis were performed in triplicates where the feasible and average value is presented with more or less one standard deviation in the Tables and Figures. The trace elements V, Sr, Y, Zr, and Pb were also analyzed utilizing the X-ray fluorescence technique (XRF) using a Philips Unique II unit fitted with an automatic sample changer PW 1510 (30 position), connected to a computer system using X-40 program for spectrometry. The detection limit of the measured elements by means of XRF technique was estimated to be 5 ppm.

In the meantime, the purity of the final obtained products of all study metal values has qualitatively been analyzed using the (ESEM-EDS) analysis. ESEM retains all the performance benefits of a traditional scanning electron microscope (SEM) but removes the high-vacuum constraint of the sample environment; Samples could be examined in their natural state without any pre-treatment.

2. 3. The leaching procedures

A series of experiments were conducted by adding a known amount of the ground ore sample (5g) to a specified volume of various leaching agents in a specified beaker. The ore slurry was stirred at the required temperature using a magnetic stirrer hotplate for the desired reaction time at a specified solid/liquid ratio. At the end of each leaching experiment, the resulting slurry was filtered and washed with lightly distilled water. The metal values of the filtrate by acid digestion were analyzed for REEs, Zn, and Ni ions to calculate their percent dissolution efficiency. The dissolution efficiency was examined according to the following Eq. (1):

$$\text{leaching efficiency } (\%) = \frac{K}{Z} \times 100 \qquad (1)$$

where K is the metal concentration in leach liquor and Z is the original metal concentration in the ore.

2.4. Data analysis and processing

MATLAB R2022a and Origin 16 software provide a very powerful tool for analysis, including plotting, simple math, statistical measures and methods, fitting FFT, peak and baseline analysis, smoothing and filtering, as well as functions for data manipulation, arrangement, and finally generation. Origin also provides graphs (including function graphs), a layout page, an Excel workbook, a matrix, and notes windows.

III. Results and discussion

3.1. Characterization of the working ore sample

The chemical composition of the working ore sample given in Table (1) reveals the predominance of Fe_2O_3, Al_2O_3, and silica, with a content of 17.16%, 19.45%, and 35.42%, respectively. On the other hand, X-ray fluorescence (XRF) analyses of some trace elements Table (1) shows that U attains 606 mg/kg besides interesting values of copper, zinc, nickel, vanadium, cadmium, and total rare earth elements with the concentration of 1500 mg/kg, 5000 mg/kg, 1761 mg/kg, 1006 mg/kg, 200 mg/kg, and 2250 mg/kg, respectively [48].

Table (1): Chemical composition of Talet Seleim ore sample.

Major oxides	**SiO_2**	**Fe_2O_3**	**Al_2O_3**	**CaO**	**MgO**	**TiO_2**	**K_2O**	**Na_2O**	**P_2O_5**	**L.O.I**	**Total**
Wt., %	35.42	17.16	19.45	1.85	3,21	0.8	1.85	0.58	0.2	18.98	99.5
Trace elements	**U**	**Cu**	**Cd**	**ΣREEs**	**Ni**	**Zn**	**Zr**	**V**	**Sr**	**Pb**	**Y**
mg/kg	606	1500	200	2250	1761	5000	163	1006	132	188	348

3. 2. Factors affecting dissolution efficiency of REEs, Zn, and Ni

The selection of the leaching agent for the dissolution of valuable elements was studied in detail using different leaching agents, followed by studying factors affecting the dissolution process.

3.2.1. Effect of acid type

The effect of different acids on the leaching efficiency of the different elements (REEs, Zn, and Ni) from the Gibbsite ore sample was studied using 150 g/L of different acids H_2SO_4, HCl, and HNO_3, with the experimental parameters set individually as follows: leaching time of 120 min, stirring speed of 200 rpm, liquid to solid ratio of 4:1, a particle size of 200 µm and temperature of 353K. Since the results in Figure (2a) show that H_2SO_4 acid has the maximum leaching efficiency, leaching systems can currently be selected based on the ease of the subsequent separation step. For this purpose, sulfuric acid leaching of the ore has some merits in terms of low process costs and efficient leaching of the metals [49-51].

3.2.2. Effect of sulfuric acid concentration

The effect of sulfuric acid concentration on the leaching efficiency of various elements was carried out under the following conditions: leaching time of 120 min, stirring speed of 200 rpm, a liquid-to-solid ratio of 4:1, a particle size of 200 µm, temperature of 353K and sulfuric acid concentration of 50, 100, 150, 200 and 250 g/L. As shown in Figure (2b), the leaching efficiencies of REEs, Zn, and Ni increased significantly but in a different manner. It can thus be mentioned that the 200 g/L sulfuric acid concentration is the optimum leaching concentration for REEs, and 150 g/L sulfuric acid concentration is the optimum leaching concentration for Zn and Ni. The leaching efficiency increased linearly with increasing the sulfuric acid concentration until it reached the optimum value. It is important to mention herein that a further increase in the acid concentration (i.e., 250 g/L) has an adverse effect on the leaching efficiencies of REEs, Zn, and Ni [52].

3.2.3. Effect of time

The effect of leaching time upon REEs, Zn, and Ni leaching efficiency from ore working sample was studied in the range from 30 to 240 min, while the other leaching conditions were fixed at 200 g/L sulfuric acid concentration, stirring speed of 200 rpm, liquid to solid ratio of 4:1, a particle size of 200 µm at a temperature of 353K. Results obtained are shown in Figure (2c), showing that as the time of leaching increased from 30 min to 240 min, the leaching efficiency increased. The leaching efficiency reached a plateau when the time increased to 240 min. From this, it can be concluded that 240 min leaching time is the optimum condition for the metal dissolution experiments.

3.2.4. Effect of liquid to solid ratio

The influence of liquid-to-solid ratio was studied by leaching mineral ore at various liquid-solid ratios and other conditions, including a sulfuric acid concentration of 200 g/L, leaching temperature of 353K, stirring

speed of 200 rpm, a particle size of 200 µm and leaching time of 240 min. Figure (2d) shows that the three metal ions have the same attitude when increasing the liquid/solid ratio from 1 to 5. The leaching efficiency was increased by the increasing liquid-solid ratio. The mass transfer driving force move metals from the solid to the liquid phase; therefore, it was increased by an increase in the liquid/solid ratio. An ideal environment for increasing the leaching efficiency of REEs, Zn, and Ni in the solution was a liquid-solid ratio of 4:1.

3.2.5. Effect of temperature

In order to study the influence of leaching temperature on the leaching efficiency of REEs, Zn, and Ni, a series of experiments were conducted under the following conditions: sulfuric acid concentration acid of 200 g /L, liquid to solid ratio of 4:1, 200 rpm stirring leaching time of 240 min, a particle size of 200 µm and leaching temperature ranging from 298 to 393K. The obtained data, which are shown in Figure (2e), indicated the importance of leaching temperature upon the study metal value leaching efficiencies from this ore material. Furthermore, the leaching rate of the three metals of REEs, Zn, and Ni was increased in a similar trend with increasing temperature from 298K to 373K, where the leaching efficiency of the three metal ions increased significantly from 43.21% to 91.88 %, 30.55 % to 89.21 % and 25.94 % to 85.25% and after which the leaching efficiency decreased with additional increases in temperature at 393K. This means that the metals leaching from the ore is an endothermic reaction [53,54].

3.2.6. Effect of stirring speed

Several tests were carried out at various mechanical stirring speeds ranging from 200 rpm to 600 rpm at 373K temperature, liquid/solid ratio of 4:1 mL/g, and sulfuric acid concentration of 200 g/L, particle size of 200 µm to explore the influence of mechanical stirring speed on metal leaching efficiency. Experimental results in Figure (2f) illustrate the significant impact that stirring speed has an appositive effect on the leaching efficiency of three different metals. The leaching efficiency of the three metal ions rose when the stirring speed was increased from 200 rpm to 400 rpm. This is brought on by a rise in the rate at which metal ions diffuse through the leaching solution. For stirring speeds above 400 rpm, a decrease was seen. This decline was attributable to the vigorous agitation that made the particles stick to the inner wall of the leaching vessel. The leaching efficiency was decreased by this phenomenon [55-57].

3.2.7. Effect of pH

The pH has a significant effect on the leaching process. Leaching experiments were carried out with pH values ranging from 0.4 to 6.0 at 373 K temperature, liquid/solid ratio of 4:1 mL/g, sulfuric acid concentration of 200 g/L, a particle size of 200 µm, and mechanical stirring speeds of 400 rpm. The findings are shown in Figure (3), where the highest leaching rate for REEs was 90.2% at pH 1.0. leaching by H_2SO_4 at pH 1.0 makes the extraction of REEs easier. The study elements leaching decreased with increasing pH value above pH 1.0. This demonstrates the dependence of leaching on the acid concentration.

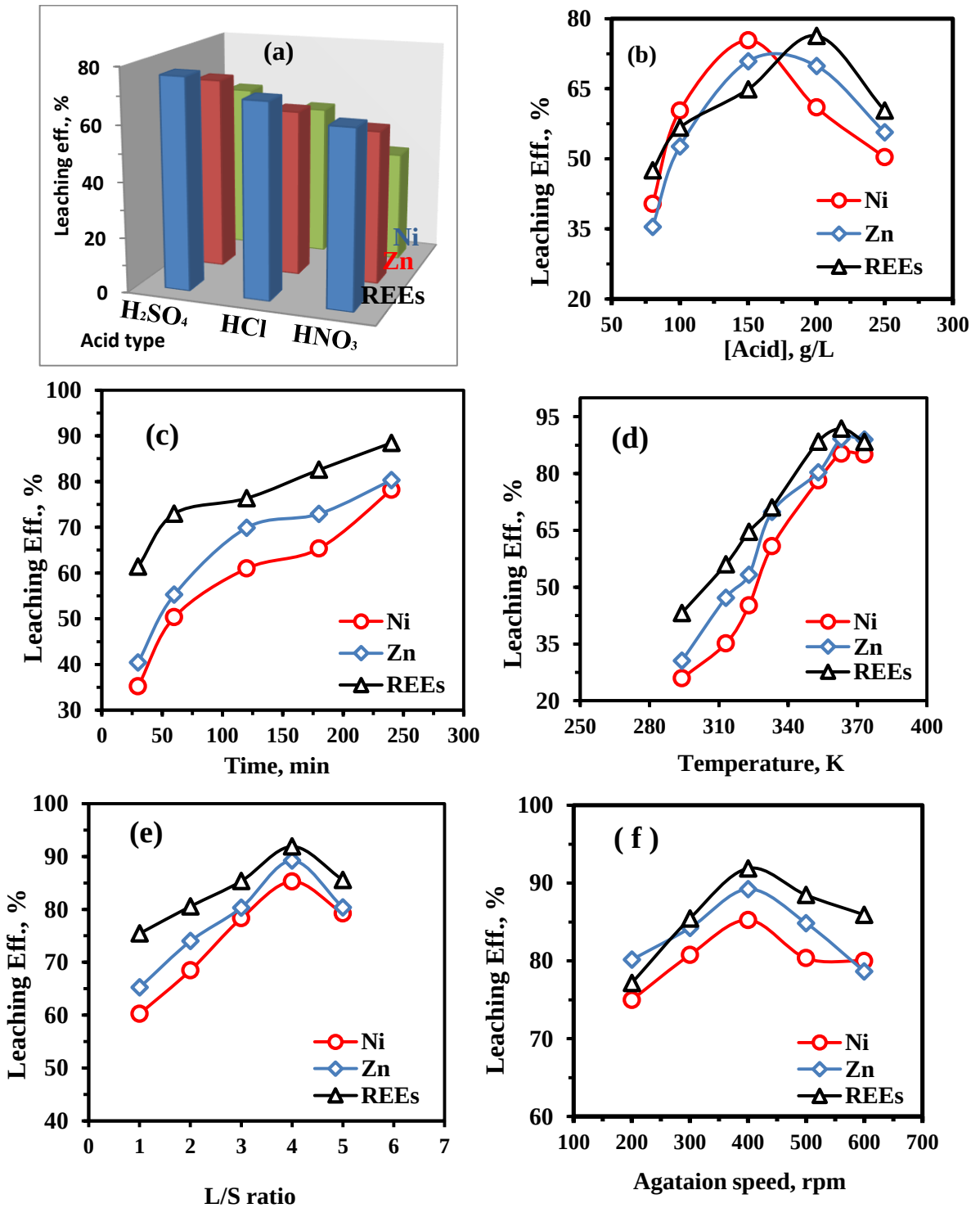

Figure (2): Effect of acid type (a), acid concentration (b), agitation time (c), temperature (d), solid/liquid ratio (e), and stirring speed (f) on leaching efficiency of REEs, Zn, and Ni from Gibbsite ore material of Talet Seleim.

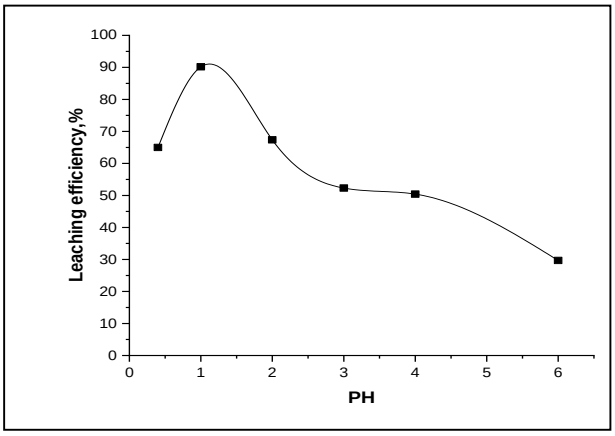

Figure (3): Effect of pH value upon leaching efficiencies of REEs, from Talet Seleim ore study sample.

From the above-studied leaching factors of the working gibbsite ore of Talet Seleim Southwestern Sinai, Egypt, it can be concluded that the optimum leaching conditions for dissolving about 91.88% REEs, 89.21% Zn, and 85.25 % Ni would be summarized in Table (2).

Table (2): optimum leaching conditions applied upon gibbsite ore material for REEs, Zinc, and Nickel leaching process.

Studied factors	Optimum conditions
Grain size	200 µm
H_2SO_4 concentration	200 g/L
Leaching time	240 min
Leaching temperature	353 K
liquid /solid ratio	4/1 mL/g
Stirring speed	400 rpm

3.3. Results of ammonium sulfate solution leaching

3.3.1. Effect of ammonium sulfate concentration

The effect of ammonium sulfate concentration on the leaching efficiency of various elements was carried out under the following conditions: leaching time of 120 min, stirring speed of 400 rpm, a liquid-to-solid ratio of 4:1, a particle size of 200 µm, temperature of 393 K, and concentration of ammonium sulfate of 100, 150, 200, 250 and 300 g/L. As shown in Figure (4a), the leaching efficiency of REEs, Zn, and Ni increased significantly in the same manner. The leaching efficiency increased linearly with increasing the ammonium sulfate concentration. Thus, it can be concluded that 250 g/L can indeed be considered an optimum value. From this value, increasing the ammonium sulfate concentration caused a lower leaching efficiency [52].

3.3.2. Effect of time

A series of experiments were conducted under the following conditions: ammonium sulfate concentration of 250 g/L, stirring speed of 400 rpm, a liquid-to-solid ratio of 4:1, a particle size of 200 µm, the temperature of 393K, and dissolution time in each test was determined to be 30, 60, 120, 180, 240 min, respectively. Figure (4b) illustrates that the leaching efficiency was increased with increasing leaching time from 30 min to 180 min. The leaching efficiency was decreased up to 180 min. From this, it can be concluded that 180 min time is the optimum condition for the metal dissolution experiments.

3.3.3. Effect of temperature

In order to study the influence of leaching temperature on the leaching of REEs, Zn, and Ni, a series of experiments were conducted under the following conditions: ammonium sulfate concentration of 250 g/L, particle size of 200 µm, a liquid-to-solid ratio of 4:1, 400 rpm stirring leaching temperature ranging from 298 to 413K and leaching time of 180 min. The results shown in Figure (4c) demonstrate that when the temperature increases, the leaching of all metals is enhanced in a similar trend. The results show that the extent of leaching efficiency of the three metal ions increased significantly from 40.12 to 90.21 %, 35.55 % to 88.98 % and 45.01 % to 85.69 % for REEs, Zn, and Ni, respectively, with increasing temperature from 298K to 413K. Although the leaching efficiency decreased with additional increases up to 393 K. Therefore, the leaching temperature was determined as 393K. In addition, this means that the metals leaching from the ore is an endothermic reaction [53,54].

3.3.4. Effect of liquid to solid ratio

The influence of liquid-solid ratio was studied by leaching mineral ore at various liquid-solid ratios and other conditions, including ammonium sulfate concentration of 250 g/L, particle size of 200 µm leaching temperature of 393K, stirring speed of 400 rpm and leaching time of 180 min ., it was found that the leaching efficiency of three metal values at L/S ratio of 5/1 has attained 90.21 % of REEs, 88.98 % of Zn, and 85.69 % Ni. So the L/S ratio of 5/1 is considered a suitable S/L ratio. The obtained results are displayed in Figure (4e).

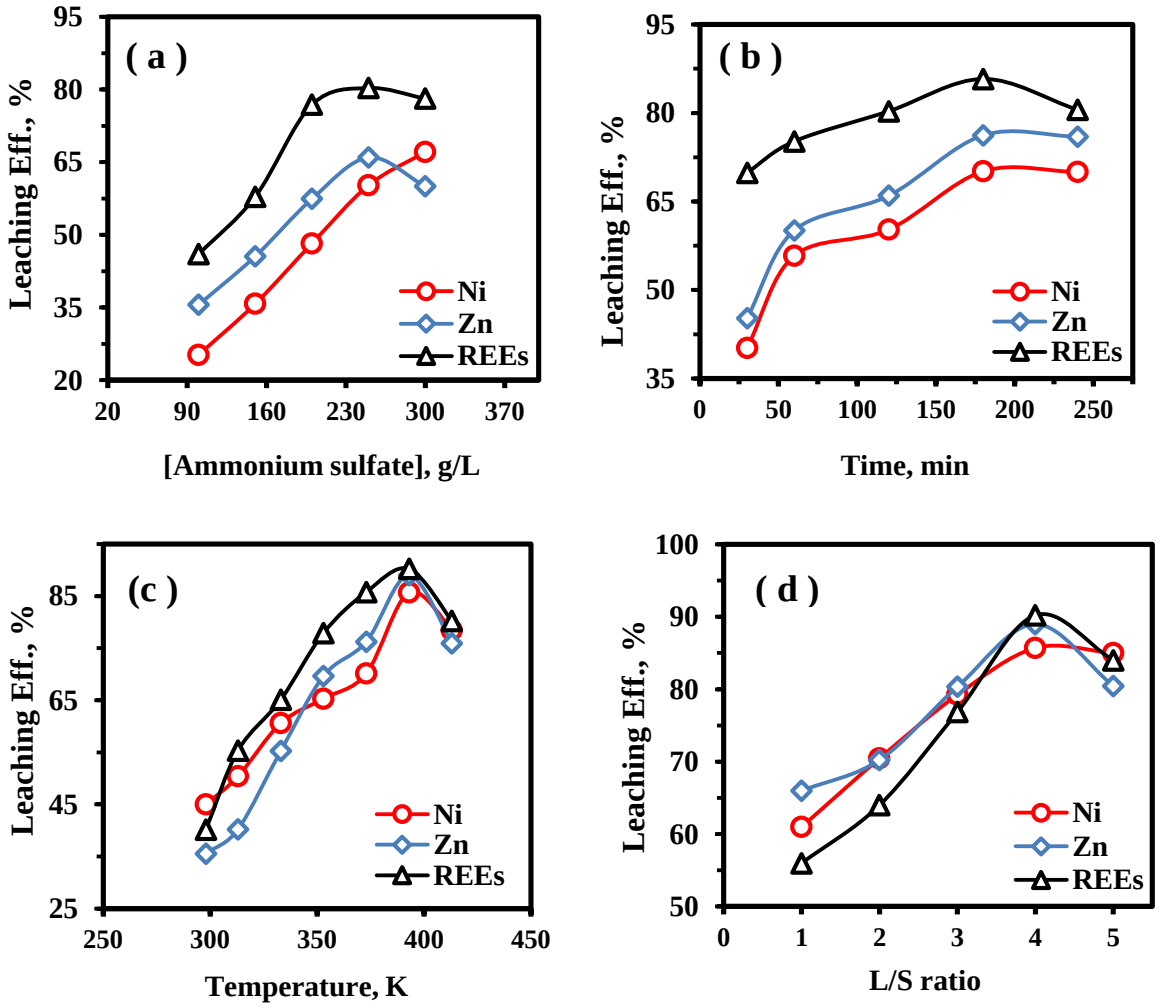

Figure (4): Effects of ammonium sulfate conc. (a), contact time (b), temperature (c), solid/liquid ratio (d) from Gibbsite ore material of Talet Seleim.

Thus, from ammonium sulfate leaching factors of the working ore sample of Talet Seleim, it may be deduced that the optimum leaching conditions for dissolving approximately 90.21 % of REEs, 88.98 % of Zn, and 85.69 % Ni are as follows: 200 µm particle size, 250 g/L of 4:1 ammonium sulfate concentration, 180 min leaching time, 5/1 L/S (liquid / solid ratio) and stirring speed 400 rpm at 393 K.

3.4. Environmentally friendly and cost-efficient

The dissolution of valuable elements in the working ore requires a temperature higher than 393 K and a concentration higher than 250 g/L; lots of ammonium gas is unavoidably released, which will deteriorate the leaching environment. Hence, a gas recovery system should be designed. In addition, excess NH_4^+ introduced through the upper concentration of ammonium sulfate must be removed or recycled to meet the discharge standard of mother leach liquor. All these requirements and devices will increase the cost. In comparison with the ammonium sulfate dissolution, the sulfuric acid dissolution consumes less leaching agent to maintain the pH value of the leaching solution system at around 1.0 and takes a lower temperature than ammonium sulfate.

3.5. Kinetics analysis of the leaching process

The kinetic analysis for the dissolution process was evaluated for the preferred leaching agents and discussed with different mathematical models.

3.5.1. Effect of leaching time at various temperatures

The effect of the reaction temperature on the rate of leaching of REEs, Ni, and Zn in the range of 298K–393K under experimental conditions of 200 µm particle size, 200 g/L with a 4/1 liquid/solid ratio, was studied. Results indicated that the leaching efficiency rate of metals increases as time and temperature increase. In order to know the kinetic model equation for the dissolution of metals, the experimental data given in Figure 5(a, b, c) were correlated to various kinetic models for solid-liquid reactions.

3.5.2. Kinetic studies and activation energy

The dissolution of three metal ions in the gibbsite ore material from Talet Seleim, Southwestern Sinai, Egypt, was applied by sulfuric acid leaching agent solution, a liquid-to-solid heterogeneous reaction. The following reaction Eq. (2) is used to illustrate the leaching reaction's stoichiometric equation symbolically:

$$H(fluid) + nD(solid) \rightarrow products \quad (2)$$

where H, D, and n refer to the fluid reactant, the solid undergoing leaching, and the stoichiometric coefficient, respectively.

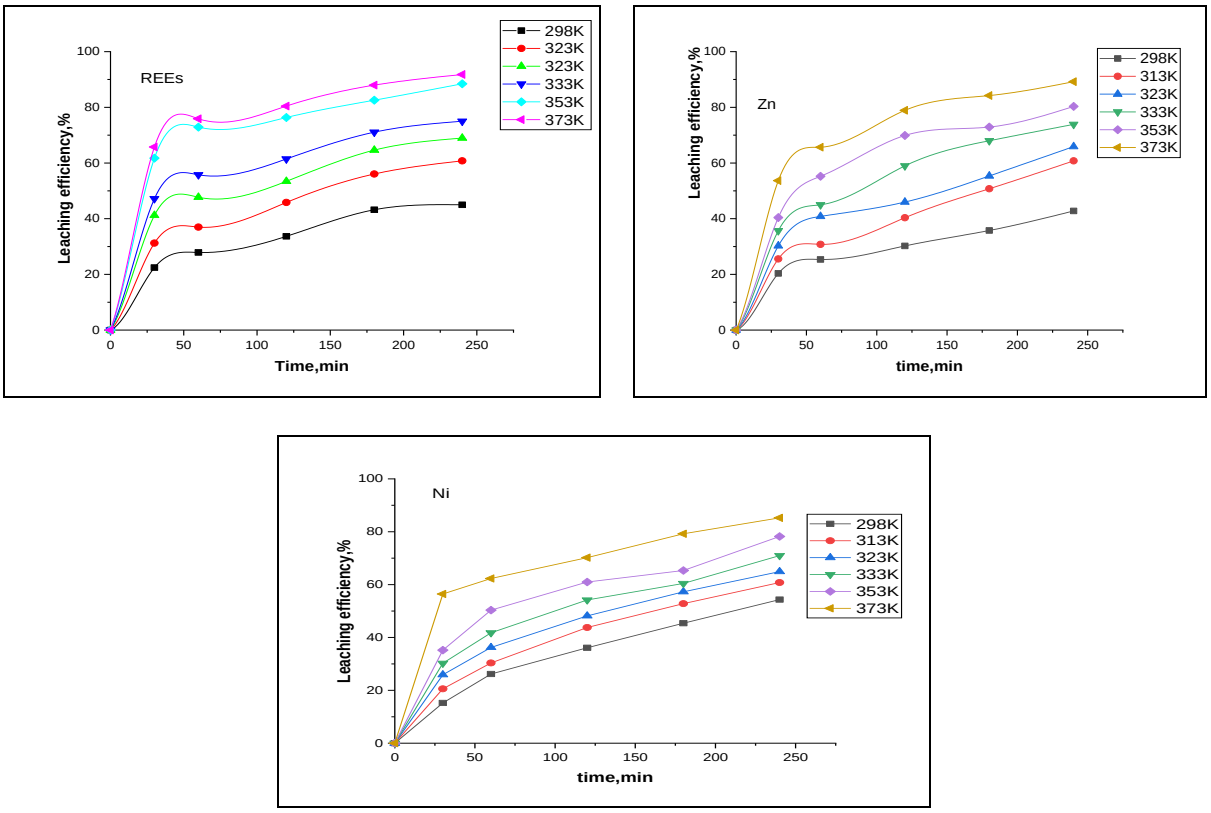

Figure (5): Effect of leaching time and temperature upon leaching efficiencies of REEs, Zn, and Ni from Talet Seleim ore study sample.

The kinetics of heterogeneous processes involving non-porous materials are commonly described using the shrinking core model (SCM). The shrinking-core model assumes that the dissolution process is controlled either by diffusion of the reactant to the surface through the diffusion layer (a liquid film), or by diffusion

through the product layer, or by a chemical reaction at the surface. The kinetics for the chemical reaction stage and the diffusion-controlled reaction can be expressed according to the following equations [58-60]:

$$\left[1-(1-G)^{1/3}\right]=k_c\,t \qquad (3)$$

$$\left[1-3(1-G)^{\frac{2}{3}}+2(1-G)\right]=k_d t \qquad (4)$$

where G is the leached fraction of three metal ions, k_c, and k_d are the rate constant of the dissolution process, and it is the leaching time in minutes.

According to Eqs. (3) and (4), when the leaching rate is controlled by the chemical reaction, the plot of $[1 - (1 - G)^{1/3}]$ vs. time is a straight line with a slope of K_c. Similar to that, the graph of $[1 -3 (1 - G)^{2/3}+2(1 - G)]$ vs. time is a straight line with a slope of K_d.

The shrinking core models with chemical reaction and diffusion via product layer as the rate-controlling processes, Eqs. (3) and (4) were assessed for the kinetic analysis in this work. $1 - (1 - G)^{1/3}$ and $[1 -3 (1 - G)^{2/3}+2(1 - G)]$ were plotted with regard to the leaching time as shown in Figures (6-7), and then the dependency of these two models on the kinetic data was evaluated using the correlation coefficient (R^2) and apparent rate constant in Tables (3) and (4).

The rate constants (K_c and K_d) are the slopes of plotting the left sides of Eqs. (3) and (4) with time. The correlation coefficients (R^2) for both chemical reaction and diffusion as the rate-controlling steps were less than 0.94. It shows that neither of the kinetic models could adequately describe how three metals in the ore were leached.

In order to examine the rate-controlling step of the solid-liquid interaction, a new form of the shrinking core model based on both interface transfer and diffusion across the product layer was developed [59]. Eq. (5) represents the integral rate expression of this model

$$^1/_3\ln(1-G)-1+(1-G)^{-1/3}=K_i t \qquad (5)$$

where K is the rate constant

In Figure 8(a, b, c), the relationship between the left side $1/3\ln (1 - G) -1+(1 - G)^{-1/3}$ and time is plotted, and the correlation coefficients R^2 are provided in Table (5). All the correlation coefficients are over 0.95. It is indicated that the model Eq. (5) can be used to describe the leaching process of REEs, Zn, and Ni in sulfuric acid solution appropriately.

For the purpose of calculating the apparent rate constants and explaining the impact of temperature with the use of Eq. (5), the values of G were fitted to shrinking sphere/core models. The logarithmic form of the Arrhenius law is used to calculate the apparent activation energy and the pre-exponential (frequency) factor (A). Using the apparent rate constants obtained by the application of Eq. (6), a plot of lnK versus 1/ T (Arrhenius plot) was shown in Figure 9(a, b, c), and the activation energy was determined as shown in Table (6). The behavior for the dissolution process of Gibbsite ore materials in Talet Seleim bornite ore is close to malachite and calcareous bornite dissolution [61] controlled by the mixing control model, where the rate-controlling step of the reaction depends on both interface transfer and diffusion across the product layer.

$$lnk = lnA - (E_a/RT) \qquad (6)$$

Where k, A, E_a, R, and T are the rate constant in min^{-1}, the pre-exponential factor, the apparent activation energy in kJ/mol, universal gas constant (8.314462 J/(mol.K), and the leaching temperature in K, respectively.

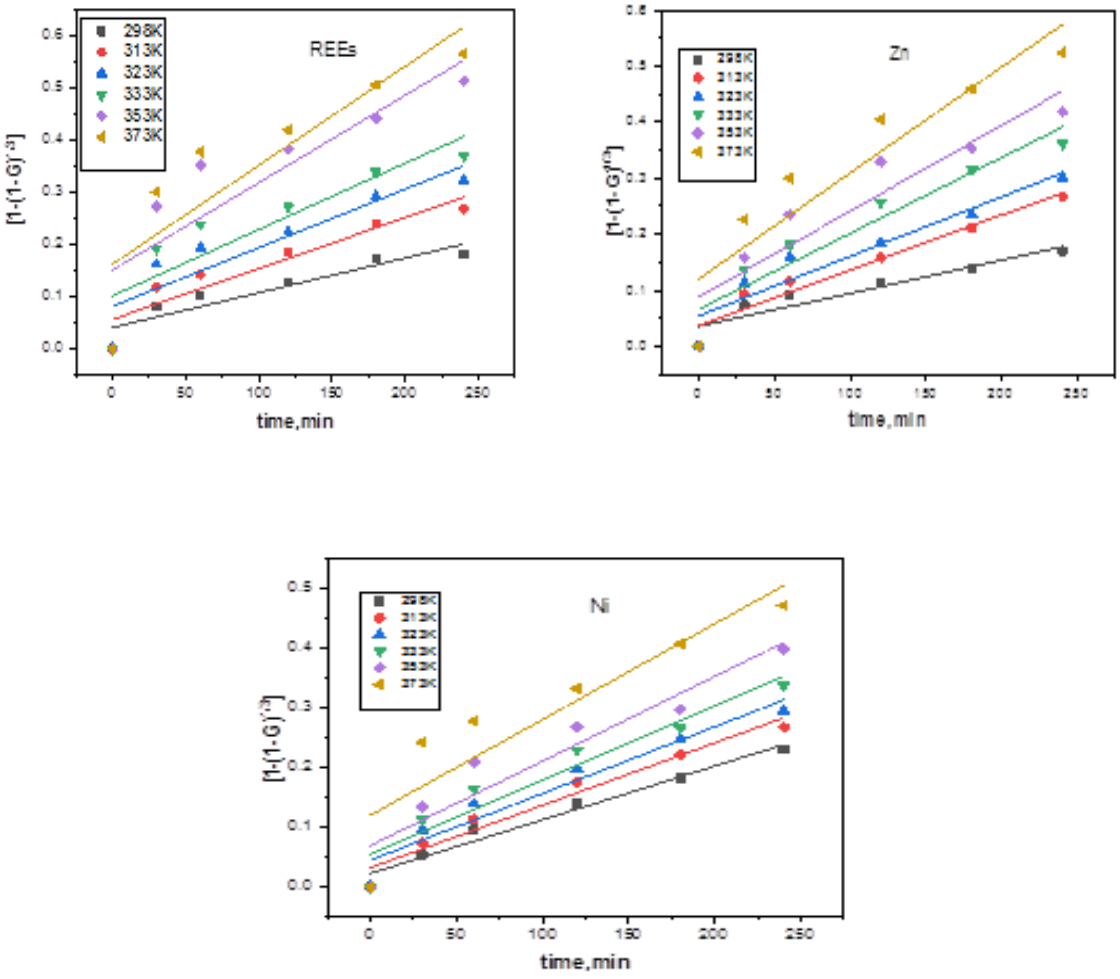

Figure (6**):** Plot of 1- (1 - G) $^{1/3}$ versus time at different temperatures for REEs, Zn, and Ni during leaching with sulfuric acid.

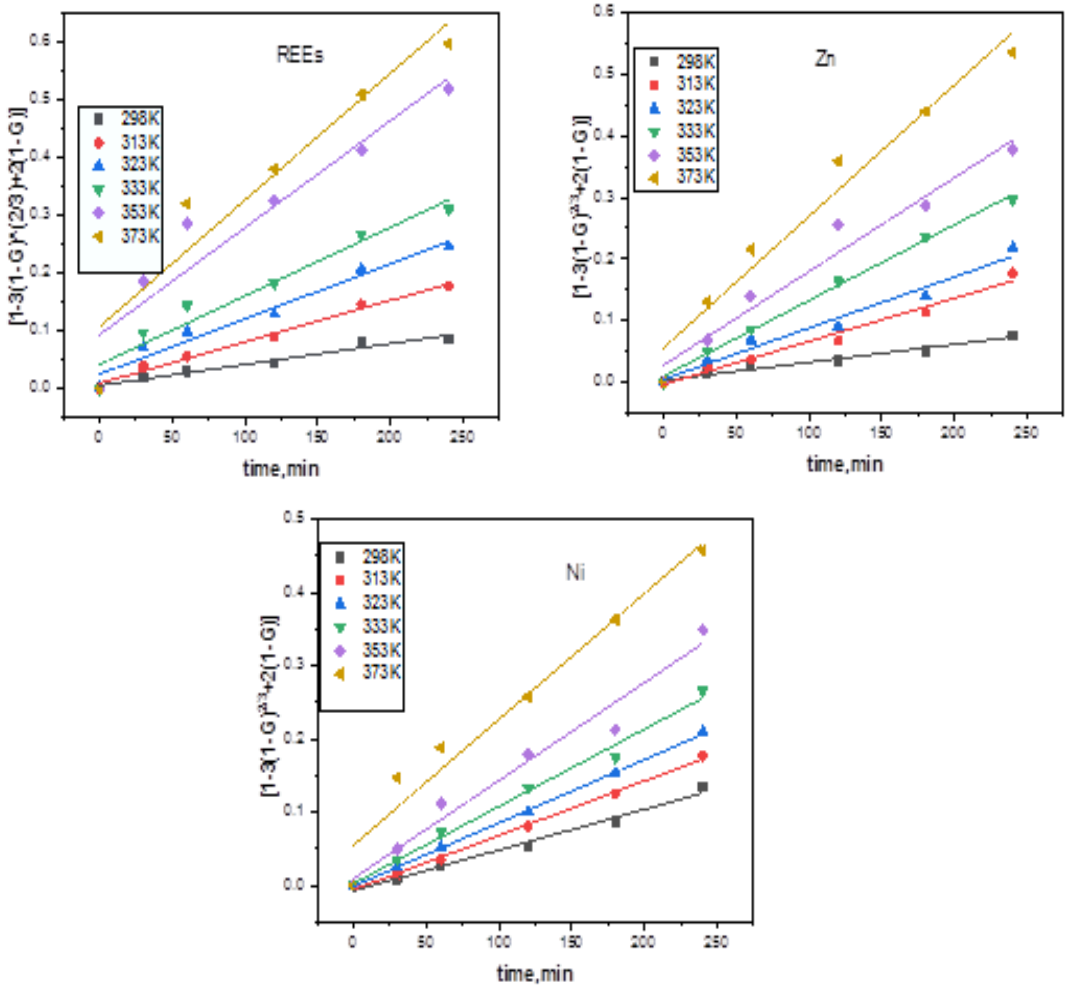

Figure (7): Plot of $1-3(1-G)^{\frac{2}{3}}+2(1-G)$ versus time at different temperatures for REEs, Zn, and Ni during leaching with sulfuric acid.

Table (3): Correlation coefficients for both chemical reaction control ash layer diffusion control model for REEs, zinc and nickel for both chemical reaction control ash layer diffusion control.

Elements	Type of reaction equation	Determination Coefficient (R^2) at different temperature					
		298K	313K	323K	333K	353K	373K
REEs	(3)	0.8569	0.8779	0.8195	0.7898	0.7457	0.7666
	(4)	0.97258	0.98931	0.96384	0.94633	0.89546	0.9059
Zn	(3)	0.86883	0.94241	0.8952	0.90599	0.86044	0.84935
	(4)	0.98038	0.97809	0.97255	0.99595	0.96454	0.96287
Ni	(3)	0.97035	0.95877	0.93547	0.92	0.8963	0.81405
	(4)	0.98563	0.99681	0.99939	0.98987	0.96947	0.95645

Table (4): Apparent rate constant (min^{-1}) based on coefficients of REEs, zinc, and nickel for both chemical reaction control ash layer diffusion control.

Elements	Eq. no	Temperature, K					
		298K	**313K**	**323K**	**333K**	**353K**	**373K**
REEs	**(3)**	6.6578×10^{-4}	9.7548×10^{-4}	1.12×10^{-3}	1.27×10^{-3}	1.68×10^{-3}	1.9×10^{-3}
	(4)	3.61243×10^{-4}	7.19371×10^{-4}	9.56303×10^{-4}	0.00119	0.00185	0.0022
Zn	**(3)**	5.90841×10^{-4}	9.84758×10^{-4}	0.00106	0.00135	0.00153	0.00189
	(4)	2.92523×10^{-4}	7.00273×10^{-4}	8.30453×10^{-4}	0.00123	0.00152	0.00213
Ni	**(3)**	8.99653×10^{-4}	0.00105	0.00112	0.00124	0.00142	0.0016
	(4)	5.54443×10^{-4}	7.41974×10^{-4}	8.63717×10^{-4}	0.00105	0.00133	0.00172

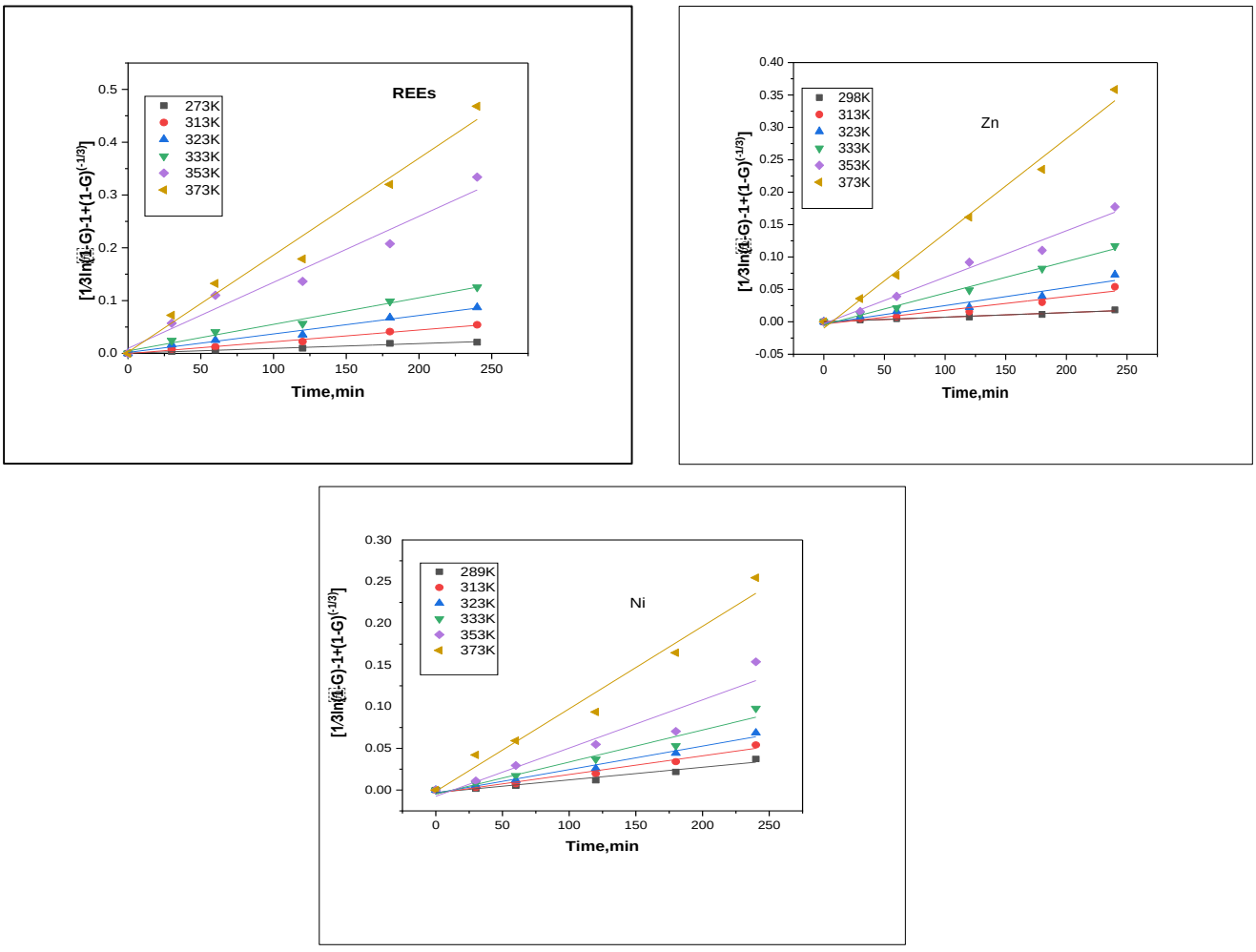

Figure (8): Plot of $1/3\ln(1 - G) - 1 + (1 - G)^{-1/3}$ versus time at different temperatures for REEs, Ni, and Zn during leaching with sulfuric acid.

Table (5): Correlation coefficients and apparent rate constant for both interfacial models for REEs, zinc, and nickel of the fitted models on the experimental data.

Elements		Temperature, K					
		298K	**313K**	**323K**	**333K**	**353K**	**373K**
REEs	k	9.08231×10^{-5}	2.23729×10^{-4}	3.50019×10^{-4}	5.03151×10^{-4}	0.00125	0.00184
	R^2	0.9762	0.9895	0.97986	0.98509	0.96128	0.97743
Zn	k	7.06282×10^{-5}	2.124×10^{-4}	2.76642×10^{-4}	4.88344×10^{-4}	7.16523×10^{-4}	0.00146
	R^2	0.97313	0.94017	0.9379	0.99201	0.98148	0.99153
Ni	k	1.51752×10^{-4}	2.24354×10^{-4}	2.81908×10^{-4}	3.84449×10^{-4}	5.78172×10^{-4}	9.89706×10^{-4}
	R^2	0.95806	0.97573	0.98142	0.9573	0.9163	0.97105

3.6. Thermodynamics characteristic of the dissolution proces

To know the feasibility and spontaneity of the leaching process as well as to understand the thermodynamic behavior of the leaching process, three metal ions are leached from an ore sample using sulfuric acid [60,62,63]. Thermodynamic parameters are evaluated by Eqs. (7) and (8):

$$\Delta G^o = -RT\ ln k_d \qquad (7)$$

$$\ln k_d = {\Delta S^o}/{R} - {\Delta H^o}/{RT} \qquad (8)$$

where the Gibbs free energy change (G°), entropy change (S°), and enthalpy change (H°) are the thermodynamic parameters. T stands for the absolute temperature in Kelvin (K), R for the gas constant (mol. K), and The equilibrium constant, denoted by k_d, can be computed using Eq. (9).

$$k_d = (C_L)/(C_S) \qquad (9)$$

where C_L represents the concentration of metal ions in a liquid solution at equilibrium in mg/L. Cs is the concentration of metal ions in a solid at equilibrium in mg/L.

According to Eq. (8), Plotting of ln k_d versus 1/T give a straight line with a slope of $-\Delta H^o$/R and the intercept of ΔS°/R as shown in Figure (10). The thermodynamic parameters were evaluated and summarized in Table (7). The positive values of enthalpy change (ΔH^o) for the three metal ions ascertained the endothermic nature of the acidic leaching in the working ore sample. Also, the positive values of entropy change (ΔS^o) for the metal ions, revealed that an increase in randomness during the leaching of metals ion. The leaching processes of REEs, Ni, and Zn were expected to be spontaneous at higher temperature and was ascertained by negative values of the Gibbs free energy change (ΔG°) as obtained in this study. The increase in the Gibbs free energy change ΔG° value with increasing temperature implies that the reaction is favorable under conditions of higher temperatures.

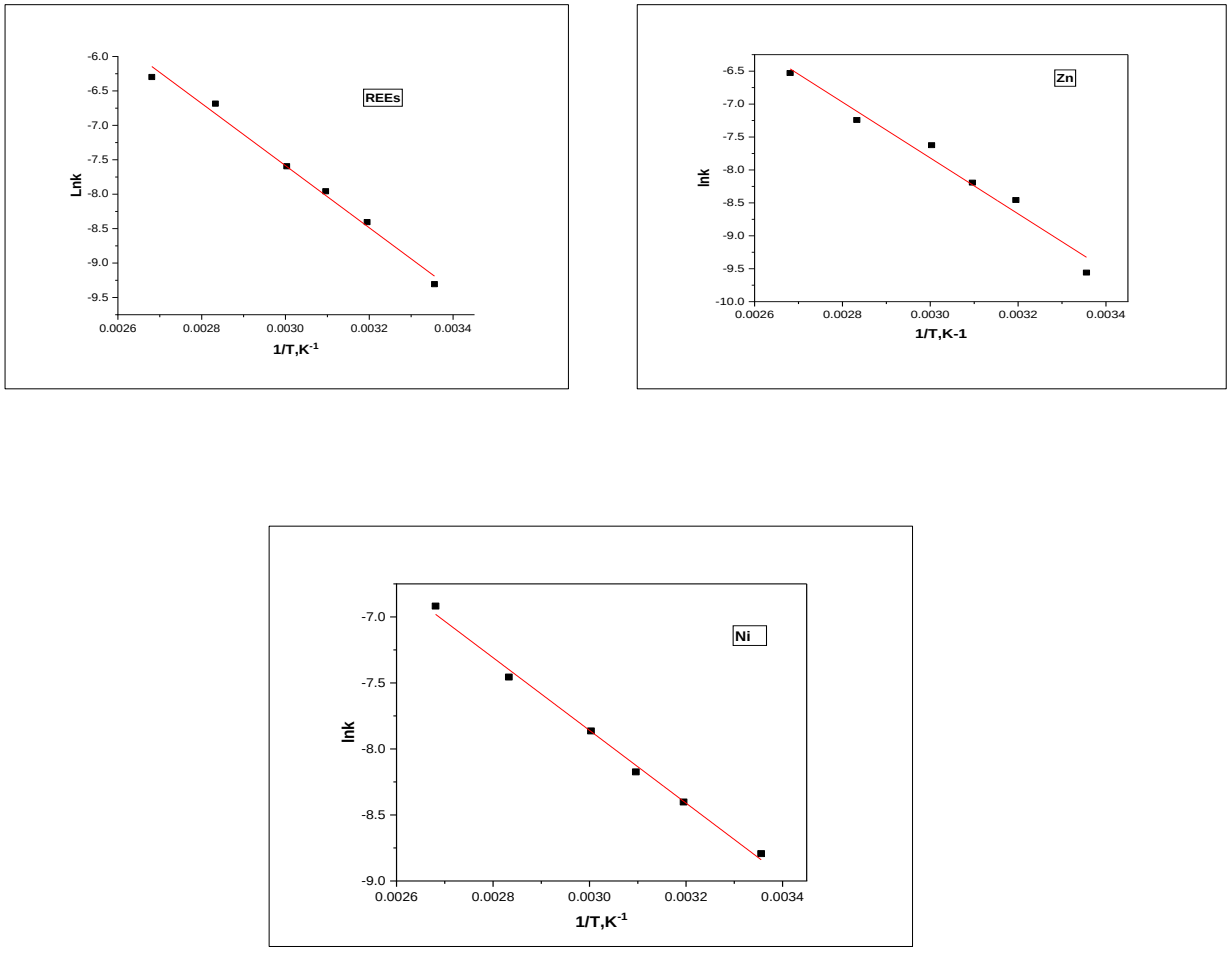

Figure (9): Plots of lnk versus reciprocal temperature of leaching REEs, Zn, and Ni during the leaching process.

Table (6): Data from Arrhenius equation for experimental data of REEs, Zn, and Ni leaching from a mineralized sample at different temperatures through the mixed interfacial model.

Metals	slope	Intercept	A	R^2	E_a
REEs	-4511.8317	5.95063	383.9952	0.98936	37.51137
Ni	-2754.89398	0.40522	1.499632	0.99483	22.9019
Zn	-4239.2500	4.89939	134.2079	0.97216	35.2451

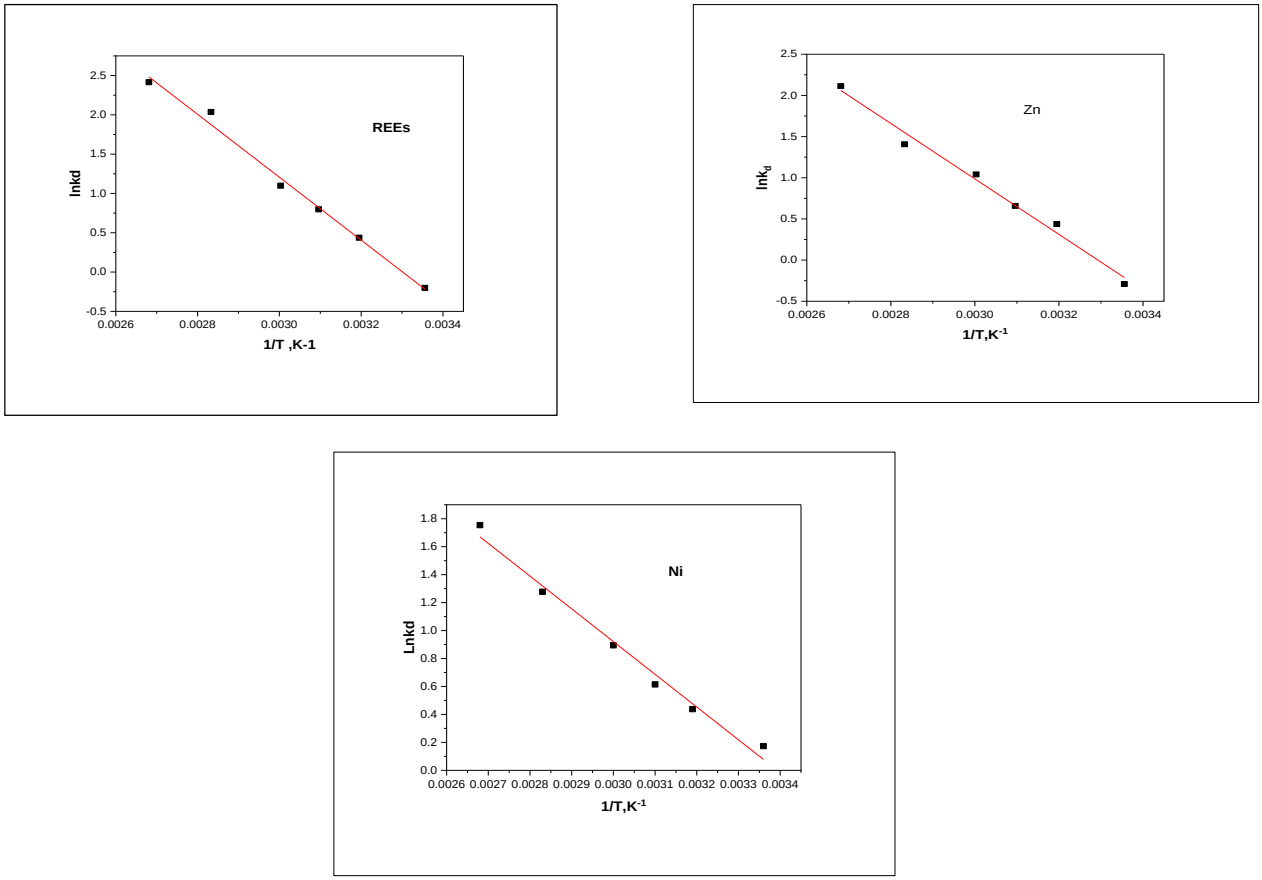

Figure (10): Plot of lnk_d versus 1/T for determination of the thermodynamic parameters of REEs, Zn, and Ni leaching in ore sample by sulfuric acid**.**

Table (7): Thermodynamic parameters for REEs, Zn, and Ni leaching from ore sample at different temperatures.

ΔG^0 (kJ/mol) and T.$\Delta S°$ (kJ/mol) at different T (K)							**ΔS^0 (kJ/mol·K)**	**ΔH^0 (kJ/ mol)**
Temp. (K)	**298**	**313**	**323**	**333**	**353**	**373**		
$\Delta G°$ (kJ/mol)								
REEs	-0.5	-1.4	-2.4	-3.01	-5.97	-7.49	0.12	33.27
Zn	0.719547	-1.1389	-1.76807	-2.88002	-4.12761	-6.55073	0.092	27.995
Ni	-0.43	-1.14	-2.40	-1.7	-1.86	-4.16	0.066	19.46968
T.$\Delta S°$ (kJ/mol)								
REEs	32.73	34.38	34.48	36.57	38.77	40.97		
Zn	27.47	28.85	29.77	30.697	32.54	34.39		
Ni	19.688	20.6789	21.3395	22.000212	23.32155	24.64288		

3.7. Results of metal values recovery

For recovering REEs, Zinc, and Nickel, a sulfate leach liquor was probably prepared by applying the optimum leaching conditions shown in Table (2) upon 1kg of the provided working ore material. This resulted in 0.5, 1.12, and 0.375 g/L within leaching efficiencies for REEs, Zn, and Ni, respectively.

3.7.1. Zinc recovery

At low pH levels, Zn should be selectively recovered as its sulfide, or ZnS (K_{sp} 2.5× 10^{-22}), from the leach liquor solution [64-66]. As opposed to metal hydroxide, zinc sulfide can be precipitated more effectively with a high metal ion recovery in a shorter retention period and at lower pH levels [64]. Using dropwise addition of 2% Na_2S solution at ambient temperature, Zn was almost fully precipitated at pH 2 according to Eq. (10).

$$ZnSO_4 + Na_2S \rightarrow ZnS \downarrow + Na_2\,SO_4 \qquad (10)$$

After solid-liquid separation by filtration, the gray ZnS precipitate was washed multiple times with distilled water to remove any contaminants. EDAX analysis was used to confirm the produced ZnS, as shown in Figure (11a).

3.7.2. Selective recovery of REEs

The leach liquor free from Zn was then subjected to selective precipitation to obtain REEs oxalates ($\mathrm{REE_s(C_2O_4)_3}$). This results from the fact that REEs form stable insoluble oxalates and can be used for their separation from solution [67]. So, oxalic acid ($C_2O_4H_2$) with a concentration of 10% was used for attaining almost complete precipitation of REEs at pH 1.1. The precipitation reaction of REEs-oxalate cake is shown by the following Eq.(11):

$$2REE_s^{3+} + 3\mathrm{H_2C_2O_4} \rightarrow \mathrm{REE_s(C_2O_4)_3} + 6\mathrm{H^+} \qquad (11)$$

The REEs-oxalate cake was then dried in a drying oven at 120 ^{o}C, followed by ignition in a muffle furnace at 850 ^{o}C for 120 min to get their oxides. The latter was subjected to EDAX semi-quantitative analysis to identify its individual REEs distribution, as demonstrated in Figure (11b).

3.7.3. Selective recovery of Ni

The solution of the ore sample was then adjusted from pH 8 to pH 12 using 20% NaOH according to the following Eq. (12) [68]. The precipitate was ignited at 850 ^{o}C for 120 min. The latter was then subjected to EDAX semi-quantitative analysis using SEM, as demonstrated in Figure (11c).

$$2\mathrm{NaOH_{(aq)}} + \mathrm{NiSO_{4(aq)}} \rightarrow \mathrm{Na_2SO_{4(aq)}} + \mathrm{Ni(OH)_{2(s)}} \downarrow \qquad (12)$$

A flow sheet for the proposed scheme for leaching process of Gibsite ore sample from talet Seleim, Southwestern, Sinai, Egypt is shown in Figure (12).

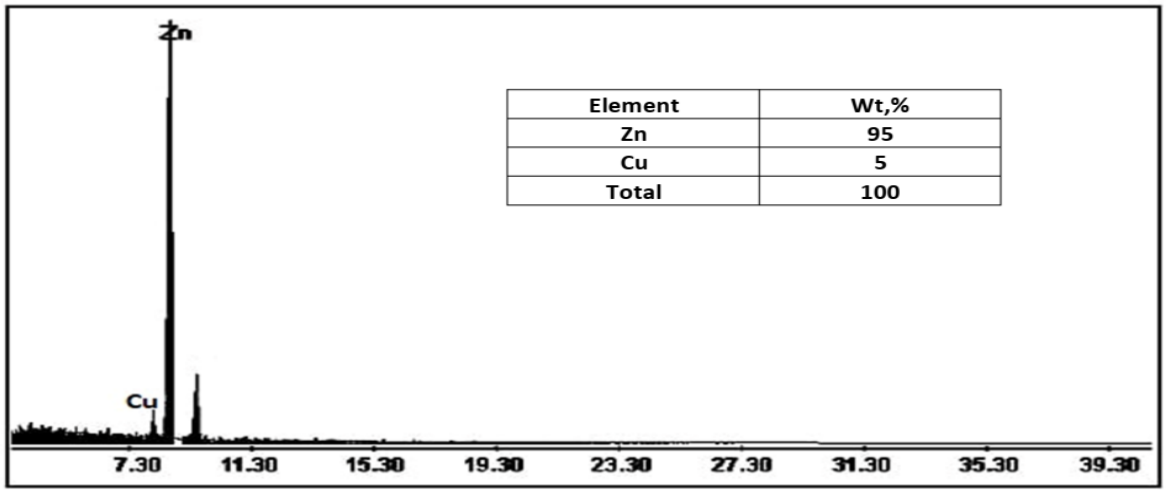

Element	Wt,%
Zn	95
Cu	5
Total	100

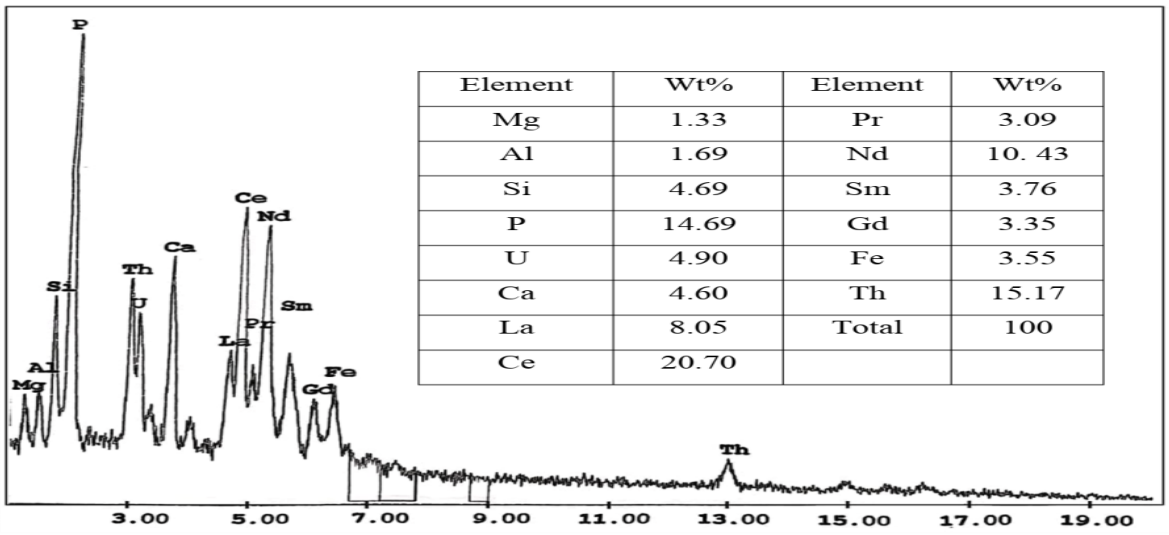

Element	Wt%	Element	Wt%
Mg	1.33	Pr	3.09
Al	1.69	Nd	10. 43
Si	4.69	Sm	3.76
P	14.69	Gd	3.35
U	4.90	Fe	3.55
Ca	4.60	Th	15.17
La	8.05	Total	100
Ce	20.70		

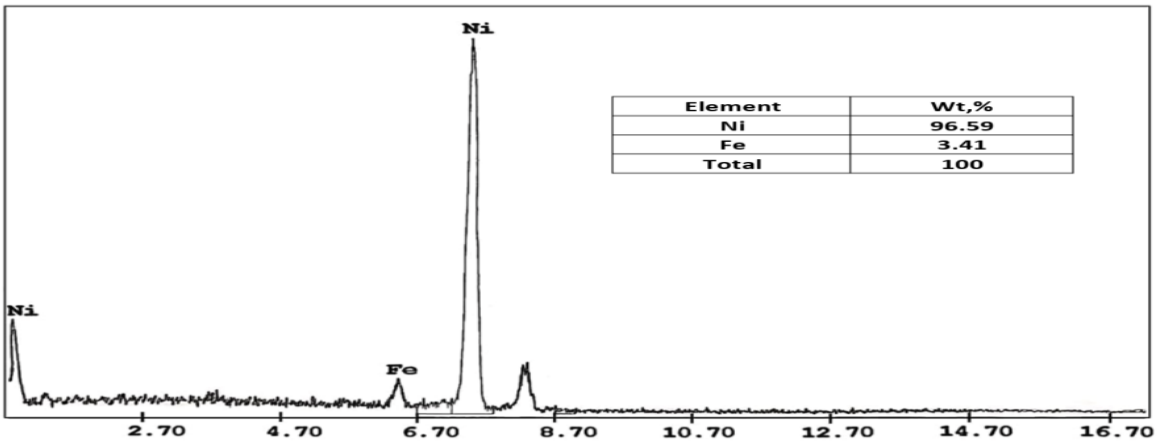

Element	Wt,%
Ni	96.59
Fe	3.41
Total	100

Figure (11): ESEM—EDX analysis of the produced (a), Zn concentrate, (b), REEs concentrate and (c), Ni concentrate..

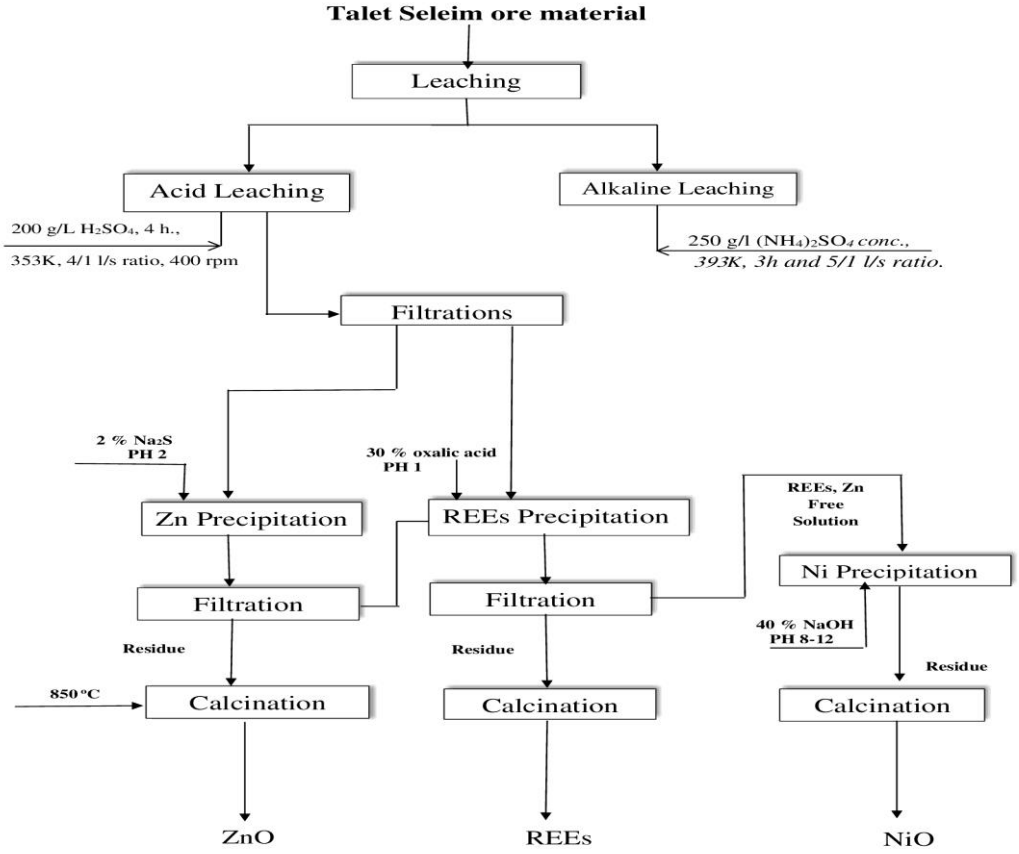

Figure (12): A flow sheet for the proposed scheme for leaching process of Gibbsite ore sample from Talet Seleim, Southwestern, Sinai, Egypt.

3.8. *Graphical nonlinear regression modeling and simulation*

There are several novel models were simulated and their validation to the leaching process were applied. Recent developments in multimedia have increased the amount of three-dimensional (3D) data that is available. Therefore, creating useful methods for their representation and processing is necessary for effective data management. Nonlinear models are increasingly preferred, not only for accuracy requirements but also for extending the use of the mode [69]. MATLAB software was adopted for a non-linear regression procedure and graphical simulation. As a result, we propose anew modeling approach that allows for quantitative non-linear representation and comparison of extended entities reciprocal spatial location in 3D space.

3.8.1 General model: General two parallel endothermic fractional n-order reactions

The general two parallel endothermic fractional n-order reactions are expressed in Eq. (13)

$$f(t,T) = qe-(a^{(1-n1)}+((n1+1)*t*(Ar1*exp(-E1*1000/(8.314*T)))))^{(1-(1-n1))}+((qe-a)^{(1-n2)}$$

$$+((n2+1)*t*(Ar2*exp(-E2*1000/(8.314*T)))))^{(1-(1-n2))} \quad (13)$$

where Ar1, Ar2, E1, and E2 are the Arrhenius constants and activation energy for the two parallel endothermic fractional n-order reactions, respectively. The sign of the reaction rate constants for the two reactions serves to identify the reversible or parallel processes. When both reactions exhibit the same signal, they are said to be

parallel; nevertheless, the presence of an opposing signal denotes the reversibility of the reactions. While nickel is reversible, zinc and REEs are parallel.

The MATLAB application was used to graph the experimental findings in 3D curves. The activation energies and correlation coefficients for the obtained results in Figure (13) demonstrate that the acidic dissolution reactions of three metals matched well with the proposed general two parallel endothermic fractional n-order reaction model and high values of correlation coefficients R^2. All MATLAB with Coefficients (with 95% confidence bounds all obtained analyzed data. The results demonstrate that a single irreversible reaction with convergent activation energy was required for the leaching of zinc. On the other hand, the rare-earth and Ni dissolution processes were carried out utilizing two separate reactions, one of which had a larger activation energy than the other. The three metal ions in the ore require an activation energy of 10-65 kJ/mol to begin their acidic digestion. REEs, Ni, and Zn react in the following order: 0.3286, 0.6439, and 0.4229, respectively. On the other hand, a different connection for the general two parallel endothermic fractional n order reactions was employed to describe the dissolution processes discovered from the group 2 experimental data (by variation of both time to temperature and the other factor fixed) model generally: Arrhenius-based two-parallel fractional reactions are included in the general shrinking core model.

3.8.2. **General Shrinking Core Model including two parallel fractional reactions with Arrhenius**

The general Shrinking Core Model includes two parallel fractional reactions with Arrhenius as expressed in Eq. (14):

$$f(X_f,T) = ((1/k_f)*Xf+(1/k_D)*(1-3*(1-X_f).\^{(2/3)} +2*(1-X_f))+(1/k_C)*(1-(1-X_f).\^{(1/3)})*(\exp(Ar_1*\exp(-E1*1000/(8.314*T)))+\exp(Ar_2*\exp(-E_2*1000/(8.314*T) \quad (14)$$

Coefficients (with 95% confidence bounds)

The resistances that can coexist in a particle undergoing reaction include chemical reaction on the surface of the unreacted core, acidic diffusion through the product layer encircling the particle, and acidic diffusion in the layer surrounding the particle. By combining these resistances, the decreasing core model used in this study was roughly resolved. The generalized shrinking core model for the dissolution process in Eq. (14) [69,70]. Where the symbols K_f, k_D, and k_C refer to the resistances to the external mass transfer, product layer diffusion, and chemical reaction, respectively, and X is the fractional conversion. As illustrated in Figure(14), the experimental data were graphed using the MATLAB program. Using the generalized shrinking core model Eq. (14) to examine the dissolution process for REEs, Ni, and Zn in 3D curves at various temperatures and times. According to the data, the activation energies for the dissolving processes for REEs, Ni, and Zn utilizing one flux were between 10 and 65 kJ/mole. For the investigated model, the computed correlation coefficients are nearer to one. The collected data features in 3D are shown in Figure (14), demonstrating that the dissolution process was controlled by film diffusion, which has the lowest value for Zn and Ni dissolution processes using sulfuric acid ($k_C > k_D > k_f$), but solid diffusion control for REEs ($k_C > k_D < k_f$). In the leaching process for the three metals, all reactions are endothermic since both values of E (E1 and E2) are negative.

3.8.3. Dissolution Kinetics according to Generalized Langmuir including liquid Solid ratio LSr and stirring speed

3.8.3.1. Generalized Langmuir including liquid Solid ratio LSr

$$\text{Langmuir equation: } q = q_m k C^n / (1 + KC)^m \quad (15)$$

The dissolution Kinetics is also simulated according to Generalized Langmuir, including liquid Solid ratio LSr and stirring speed, as shown in Eq.(16).

General model: Generalized Langmuir including liquid Solid ratio LSr

$$f(LSr, C) = q_m * k * LSr^m * C^n/(1 + k * LSr^f * C^e)^g \quad (16)$$

Coefficients (with 95% confidence bounds)

The Generalized Langmuir, including the liquid-solid ratio, mL/g, is shown in Figure (15).

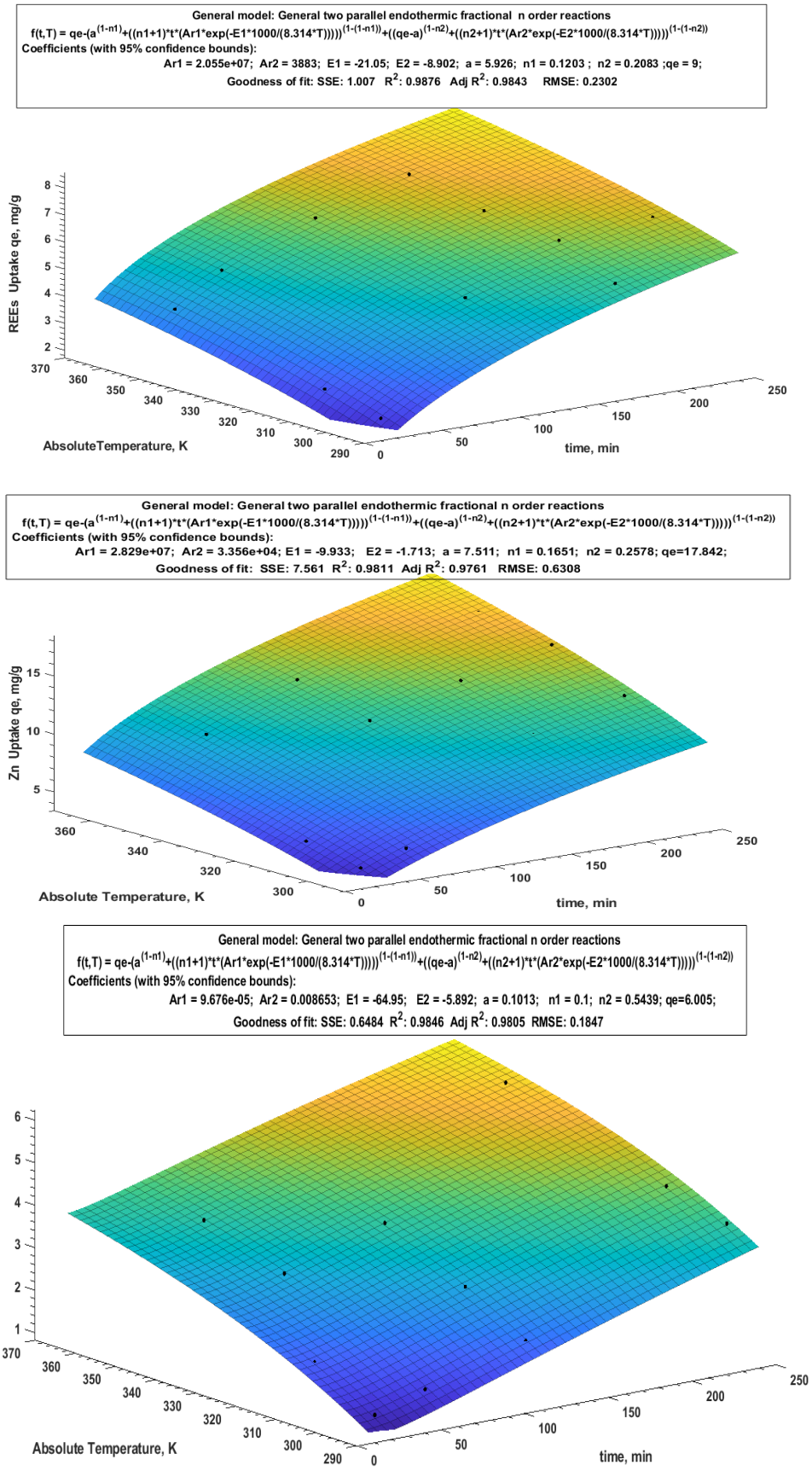

Figure (13): Generalized two parallel endothermic fractional n order reactions general model.

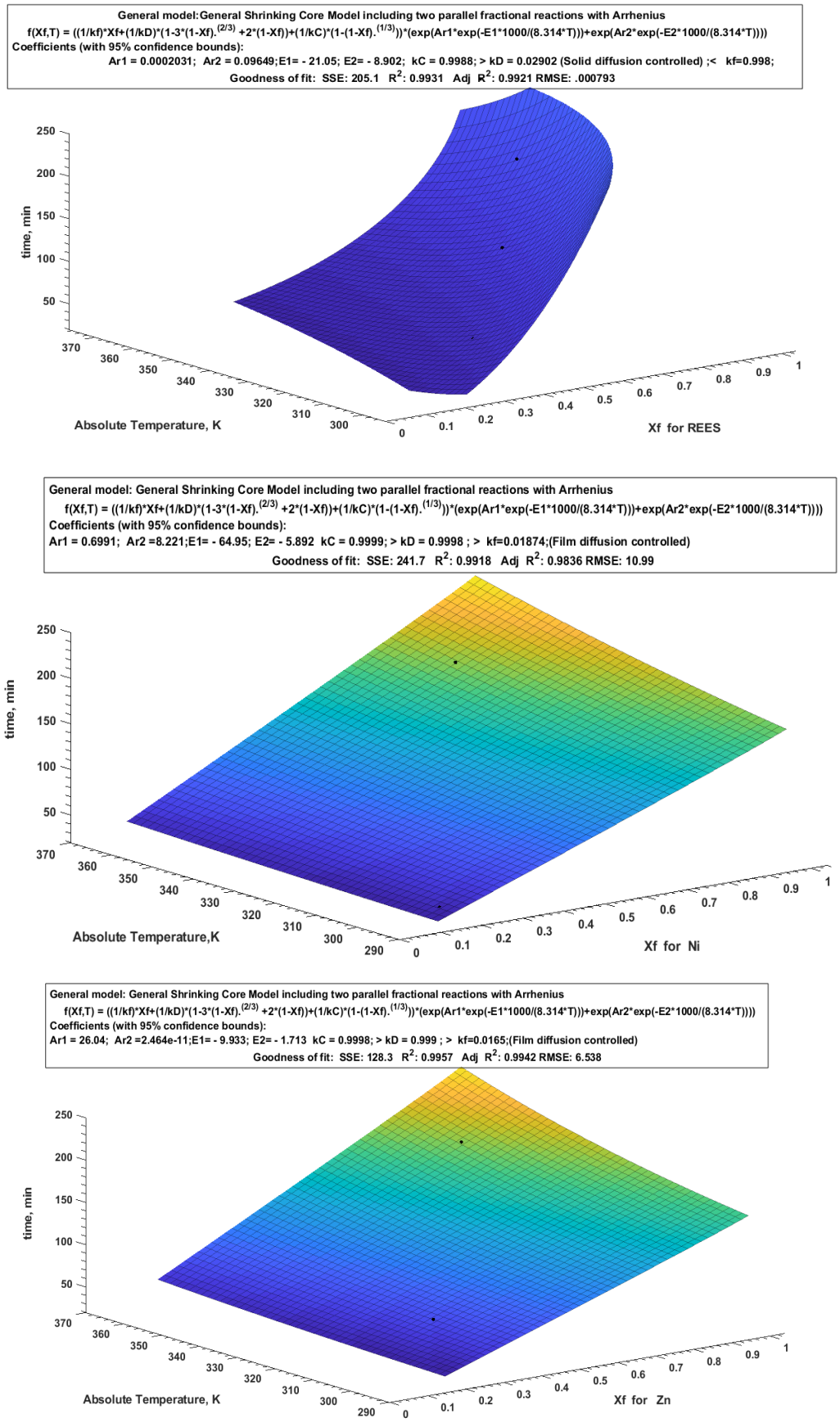

Figure (14): Generalized Shrinking Core Model including two parallel fractional reactions with Arrhenius.

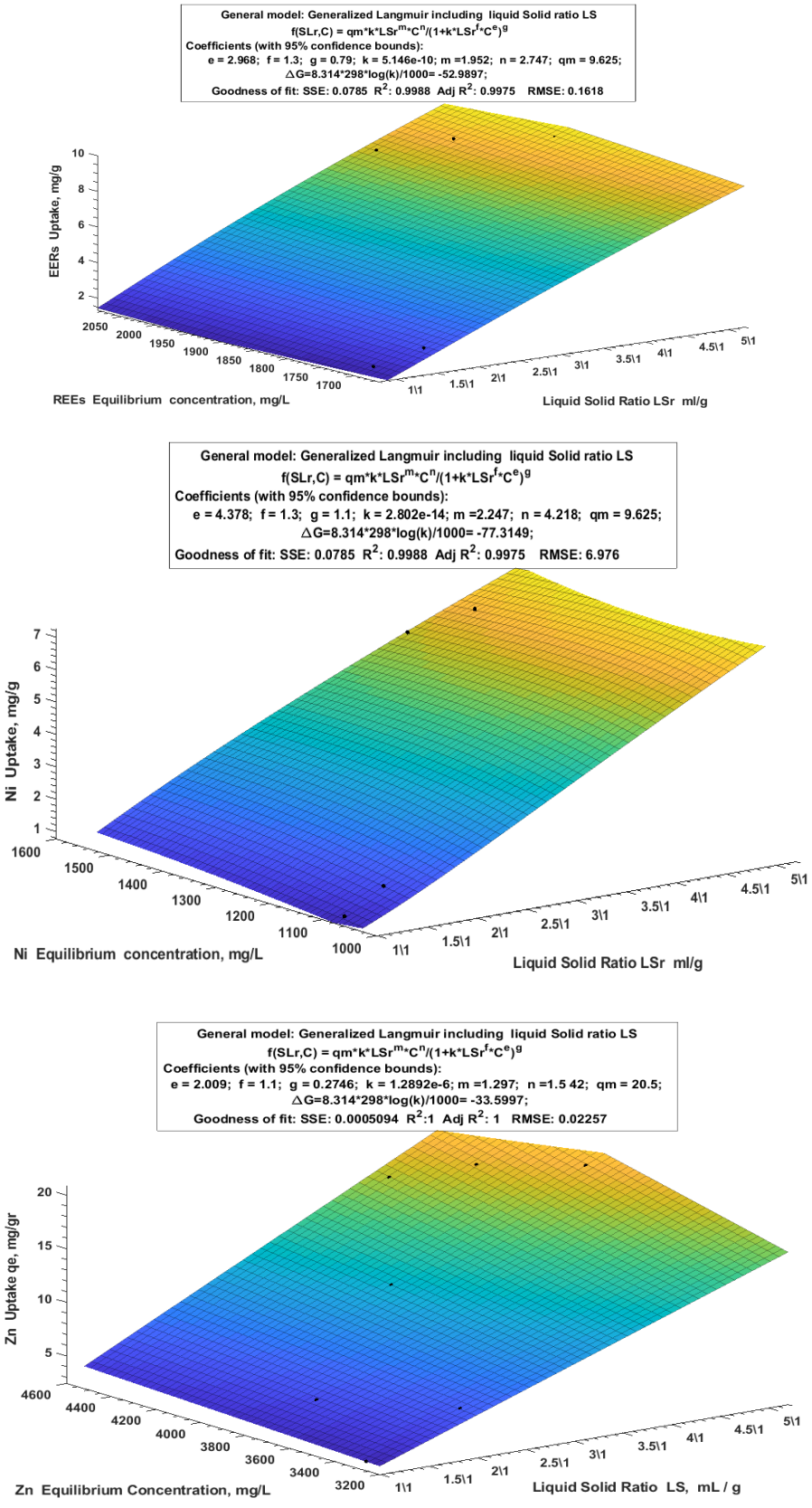

Figure (15): Generalized Langmuir including liquid solid ratio, ml/g

3.8.3.2. Generalized Langmuir, including stirring speed

The relation between the uptake of metals versus stirring speed during the leaching process. Are shown in Figure (16) by the generalizing Langmuir Eq. (17), including stirring speed;

$$\mathrm{f(rpm, C)} = q_m * k * \mathrm{rpm}^m * C^n/(1 + k * \mathrm{rpm}^f * C^e)^g \qquad (17)$$

where rpm is stirring speed and e, f, g, k, m, and n exponentials are the parameters constants powers. Using the systematic approach presented in Eq. (17) using the results of the uptakes at different stirring speeds and different initial concentrations, experimental data have been graphed using the MATLAB program in 3D (surfaces) and presented in Figure (16). By applying the nonlinear equation of the general Langmuir isotherm model Eq. (15) can express several relations in the 3D by using the MATLAB program. Practically, in general, the leaching processes for all three metal ions have a better association with experimental profiles: qm, R2, and Adj R2 values, and fast statistical terms confirm this analysis. All the MATLAB models are with 95% confidence bounds. Figure (16) clearly demonstrates that the order of function-power: the higher order of exponentials magnitude, the more reaction dependence on the stirring speed, initial concentration, and (rpm × C). The values of power constant parameters provide information for describing these sorption systems. The m constant (rpm m) indicates that the rpm is the most effective factor in the leaching process. While the n constant (C^n), indicates that the C_0 is the second effective factor. Finally, the product of (f × g) for rpm and (e × g) in $rpm \times C^e)^g$ part can be compared with the m and n values to show the degree of their effect. The results indicate that their effect together is limited: M > f >n >e >g.

Gibbs Free energy change (ΔG, in kJ.mol^{-1}) is related to *K* (the Langmuir constant) by the equation: ΔG=8.314×298*log(k)/1000; R is the gas constant (8.314J·K^{-1}·mol^{-1}), and T is the absolute temperature. The negative free energy ΔG values are: -52.9897, -77.3149, and -33.5997kJ mol^{-1} k^{-1} for REEs, Ni, and Zn, respectively, at 298 K. ΔG values are similar trend and consistent with experimental observations for the ΔG values from thermodynamics. The liquid-solid ratio (LSr) was used to validate the simulated generalized Langmuir to it. The values of thermodynamic parameters are consistent with experimental observations for the ΔG values from thermodynamics and are the same in the other model.

3.8.4. Thermodynamic Characteristics

The non-linear Floatotherm (anisotherm) was suggested as a result of the temperature variation for all three metals during the acidic leaching process [69,70]. A suggested Floatotherm (an isotherm) Van't Hoff equation Eq. (18) was derived as follows [69,70].

$$F(C,T) = qm*(\exp(-\Delta H*1000/(RT)+\Delta S/R))*C^n/(1+(\exp(-\Delta H/(RT)+\Delta S/R))*C^m)^g \qquad (18)$$

n and m practically tend to be equal. The proposed model was visualized in 3D using MATLAB as shown in Figure (17) K_d (ml/g), ΔH (KJ/mol), ΔS (J/mol.K), T (Kelvin), and R (KJ/K.mol) stand for the distribution coefficient, enthalpy, entropy, temperature in Kelvin, and molar gas constant, respectively. The possibility and spontaneous character of the breakdown processes are confirmed by the negative value of the free energy of digestion (ΔG). As a result, it was discovered that the adsorption process was endothermic and spontaneous. When the sulfuric acid attacked the ore particles, the Δ S values showed a positive value, indicating an increase in randomness at the solid/solution interface. DH, DS, DG, and are used instead of ΔH, ΔS, and ΔG to avoid MATLAB coding confusing. The positive value of ΔH confirming the endothermic nature of the dissolution process for the three metals.

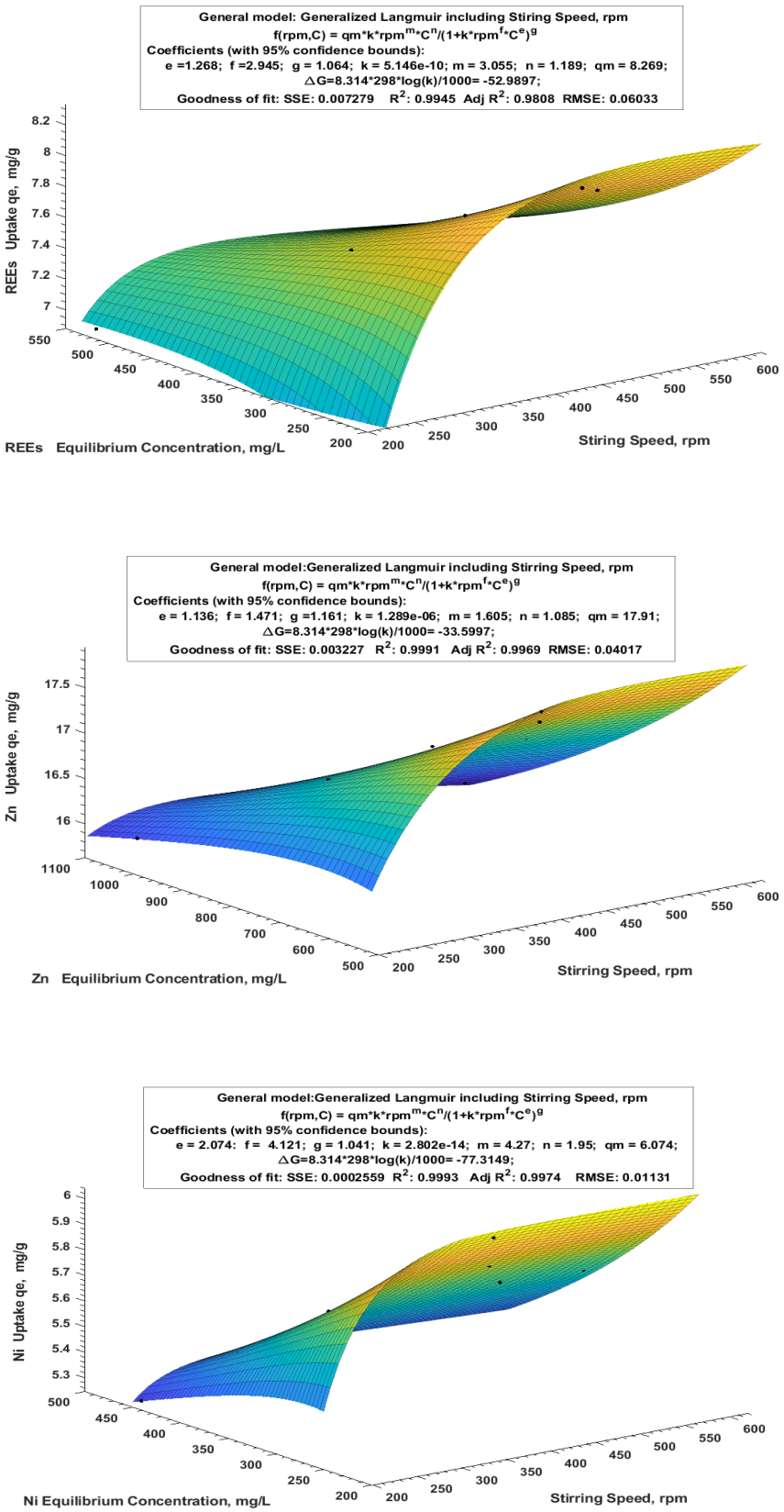

Figure (16): Parameters of generalized Langmuir including stirring speed rpm for REEs, Zn and Ni.

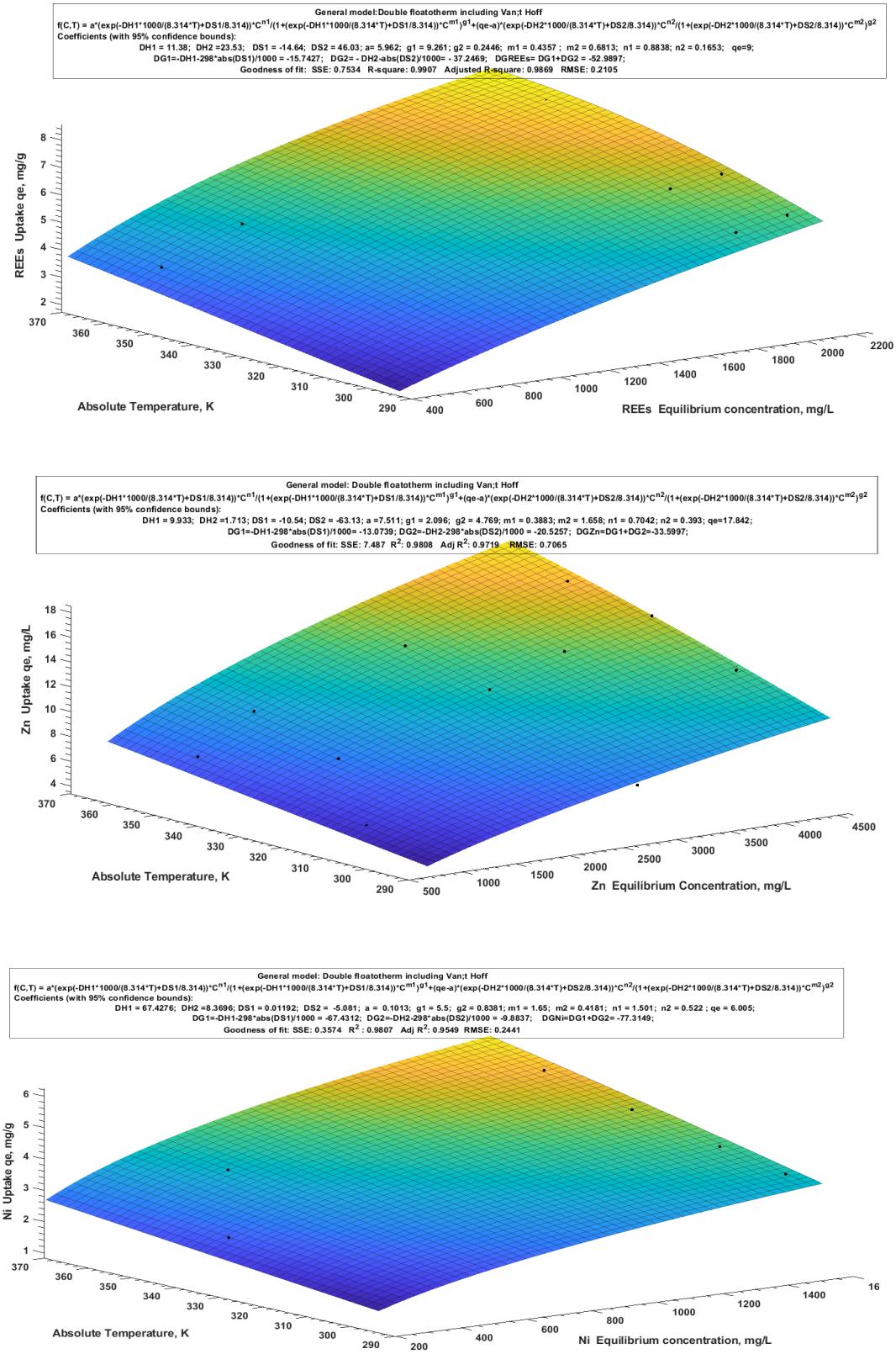

Figure (17): General model Double floatotherm including Vant Hoff for REEs, Zn, and Ni.

IV. Conclusions

In this study, the kinetics of REEs, Ni and Zn leaching from gibbsite ore in a sulfuric acid solution was investigated. The study research showed that the leaching efficiency of three metal ions increased with the sulfuric acid concentration, solid-liquid ratio, and reaction temperature. Under the most favorable conditions of acid concentration = 200 g/L, liquid-to-solid phase ratio = 4/1, time = 240 min, particle size = 200µm, temperature = 353K, and the effect of stirring speed is 400 rpm. The leaching efficiency dissolved about 91.88 % REEs, 89.21% Zn, and 85.25 % Ni. In case of ammonium sulfate leaching the results of REEs, Zn and Ni were 90.21 %, 88.98 %, and 85.69 % Ni, respectively at 200 µm particle size, 250 g/L of 4:1 ammonium sulfate concentration, 180 min leaching time, 5/1 L/S (liquid / solid ratio) and stirring speed 400 rpm at 393 K. The leaching with sulfuric acid is better than the ammonium sulfate leaching process. The dissolution kinetics of three metal ions in this study is controlled by both the interface transfer and diffusion across the product layer of ore. This model equation is given as $1/3\ln(1 - G) - 1 + (1 - G)^{-1/3} = K_i t$. The activation energy was evaluated to be 37.51, 22.90, and 35.25 kJ/mol for REEs, Ni, and Zn, respectively. Also, thermodynamic studies showed that the leaching process is endothermic. The positive values of ΔH^o and ΔS^o of metal ions ascertained the endothermic nature of the acidic dissolution and the increase in the randomness during the dissolution process in the gibbsite ore. The increase in $\Delta G°$ value with increasing temperature suggests that the dissolution reaction is more favorable at a higher temperature. In order to recover the metal ions of interest, it can be stated that H_2SO_4 acid leaching is more favored for preparing the pregnant leach liquid (REEs, Zn, and Ni). Finally, a flow sheet was created using the collected data.

Future perspective:

In the future, we are interested in further improvements in the dissolution method for metals and the selectivity of the REEs, zinc and nickel dissolution process to develop optimum conditions for 100% recovery of each metal, in addition to recovery of metals with the different techniques.

Compliance with ethical standards

Conflict of interest There is no conflict of interest in this work.

References

[1]. El-Sheikh EM, Ghazala RA, Abdelwarith A, Salem F, Ali S (2015) Leaching Characteristics of Uranium And Copper from Their Mineralization in the Carbonate Rich latosol of Abu-Thor Locality, South Western Sinai, Egypt. Isotope and Radiation Research 47:231-246

[2]. El Hazek MN, Ahmed FY, El Kasaby MA, Attia RM (2008) Sulfuric acid leaching of polymetallic Abu Zeneima gibbsite-shale. Hydrometallurgy 90:34-39. https://doi.org/https://doi.org/10.1016/j.hydromet.2007.09.009

[3]. Orabi AH, El-Sheikh EM, Saleh WH, El-Saied FA, El-Gendy HS, Ismaiel DA (2019) Recovery of uranium and copper from mineralized dolostone, Gabal Allouga, Southwestern Sinai, Egypt. Journal of Radiation Research and Applied Sciences 12:10-23. https://doi.org/https://doi.org/10.1080/16878507.2019.1594095

[4]. Zaki DI (2021) Recovery of Uranium, Copper, and Zinc from Abu Thor Gibbsite Bearing Shale Ore Material, Abu Zeneima Area, Southwestern Sinai, Egypt. Radiochemistry 63:724-733. https://doi.org/10.1134/S1066362221060035

[5]. Shayesteh K, Abbasi P, Vahid Fard V, Shahedi Asl M (2020) Simultaneous Removal of Nickel and Cadmium During the Cold Purification of Zinc Sulfate Solution. Arabian Journal for Science and Engineering 45:587-598. https://doi.org/10.1007/s13369-019-04320-9

[6]. Park K-H, Nam CW (2008) Status and prospect of nickel resources and processing. Trending Metals and Materials Engineering 21:1-9. https://doi.org/10.1007/978-0-387-09545-5_1

[7]. Li J, Li D, Xu Z, Liao C, Liu Y, Zhong B (2018) Selective leaching of valuable metals from laterite nickel ore with ammonium chloride-hydrochloric acid solution. Journal of Cleaner Production 179:24-30. https://doi.org/https://doi.org/10.1016/j.jclepro.2018.01.085

[8]. Crundwell FK, Moats MS, Ramachandran V, Robinson TG, Davenport WG (2011) Chapter 1 - Overview. In: Crundwell FK, Moats MS, Ramachandran V, Robinson TG, Davenport WG (eds) Extractive Metallurgy of Nickel, Cobalt and Platinum Group Metals. Elsevier, Oxford, pp 1-18. https://doi.org/https://doi.org/10.1016/B978-0-08-096809-4.10001-2

[9]. Ribeiro PPM, dos Santos ID, Neumann R, Fernandes A, Dutra AJB (2021) Roasting and Leaching Behavior of Nickel Laterite Ore. Metallurgical and Materials Transactions B 52:1739-1754. https://doi.org/10.1007/s11663-021-02141-6

[10]. Meshram P, Abhilash, Pandey BD (2019) Advanced Review on Extraction of Nickel from Primary and Secondary Sources. Mineral Processing and Extractive Metallurgy Review 40:157-193. https://doi.org/10.1080/08827508.2018.1514300

[11]. Li B, Ding Z, Wei Y, Wang H, Yang Y, Barati M (2018) Kinetics of Reduction of Low-Grade Nickel Laterite Ore Using Carbon Monoxide. Metallurgical and Materials Transactions B 49:3067-3073. https://doi.org/10.1007/s11663-018-1367-8

[12]. Thubakgale CK, Mbaya RKK, Kabongo K (2013) A study of atmospheric acid leaching of a South African nickel laterite. Minerals Engineering 54:79-81. https://doi.org/https://doi.org/10.1016/j.mineng.2013.04.006

[13]. Doggett M (2022) Mineral Economics and the Business of Mineral Supply. SEG Discovery:25-39. https://doi.org/10.5382/Geo-and-Mining-17

[14]. Cao S, Chang L, Bi X, Luo S, Liu J (2022) The Extraction of Silica from Nickel Laterite Ore by Alkaline Hydrothermal Process. Mining, Metallurgy & Exploration 39:1245-1253. https://doi.org/10.1007/s42461-022-00597-x

[15]. Mineral Commodity Summaries 2019 (2019). Mineral Commodity Summaries. Reston, VA. https://doi.org/10.3133/70202434

[16]. Eksteen JJ, Oraby EA, Nguyen V (2020) Leaching and ion exchange based recovery of nickel and cobalt from a low grade, serpentine-rich sulfide ore using an alkaline glycine lixiviant system. Minerals Engineering 145:106073. https://doi.org/https://doi.org/10.1016/j.mineng.2019.106073

[17]. Zevgolis EN, Daskalakis KA (2021) The Nickel Production Methods from Laterites and the Greek Ferronickel Production among Them. Materials Proceedings 5 (1). https://doi.org/10.3390/materproc2021005104

[18]. Ribeiro PPM, de Souza LCM, Neumann R, dos Santos ID, Dutra AJB (2020) Nickel and cobalt losses from laterite ore after the sulfation-roasting-leaching processing. Journal of Materials Research and Technology 9:12404-12415. https://doi.org/https://doi.org/10.1016/j.jmrt.2020.08.082

[19]. Liu X, Huang J, Zhao Z, Chen X, Li J, He L, Sun F (2023) Nickel leaching kinetics of high-grade nickel matte with sulfuric acid under atmospheric pressure. Hydrometallurgy 215:105987. https://doi.org/https://doi.org/10.1016/j.hydromet.2022.105987

[20]. Xiao W, Chen X, Liu X, Zhao Z, Li Y (2021) A method for extracting valuable metals from low nickel matte by non-oxidative leaching with H2SO4. Separation and Purification Technology 270:118789. https://doi.org/https://doi.org/10.1016/j.seppur.2021.118789

[21]. Pandey N, Tripathy SK, Patra SK, Jha G (2022) Recent Progress in Hydrometallurgical Processing of Nickel Lateritic Ore. Transactions of the Indian Institute of Metals. https://doi.org/10.1007/s12666-022-02706-2

[22]. Whitworth AJ, Vaughan J, Southam G, van der Ent A, Nkrumah PN, Ma X, Parbhakar-Fox A (2022) Review on metal extraction technologies suitable for critical metal recovery from mining and processing wastes. Minerals Engineering 182:107537. https://doi.org/https://doi.org/10.1016/j.mineng.2022.107537

[23]. Johnson JA, Cashmore BC, Hockridge RJ (2005) Optimisation of nickel extraction from laterite ores by high pressure acid leaching with addition of sodium sulphate. Minerals Engineering 18:1297-1303. https://doi.org/https://doi.org/10.1016/j.mineng.2005.05.013

[24]. He F, Ma B, Wang C, Zuo Y, Chen Y (2022) Dissolution behavior and porous kinetics of limonitic laterite during nitric acid atmospheric leaching. Minerals Engineering 185:107671. https://doi.org/https://doi.org/10.1016/j.mineng.2022.107671

[25]. McDonald RG, Whittington BI (2008) Atmospheric acid leaching of nickel laterites review: Part I. Sulphuric acid technologies. Hydrometallurgy 91:35-55. https://doi.org/https://doi.org/10.1016/j.hydromet.2007.11.009

[26]. McDonald RG, Whittington BI (2008) Atmospheric acid leaching of nickel laterites review. Part II. Chloride and bio-technologies. Hydrometallurgy 91:56-69. https://doi.org/https://doi.org/10.1016/j.hydromet.2007.11.010

[27]. Rice NM (2016) A hydrochloric acid process for nickeliferous laterites. Minerals Engineering 88:28-52. https://doi.org/https://doi.org/10.1016/j.mineng.2015.09.017

[28]. Xu H, Wei C, Li C, Fan G, Deng Z, Zhou X, Qiu S (2012) Leaching of a complex sulfidic, silicate-containing zinc ore in sulfuric acid solution under oxygen pressure. Separation and Purification Technology 85:206-212. https://doi.org/https://doi.org/10.1016/j.seppur.2011.10.012

[29]. Ejtemaei M, Gharabaghi M, Irannajad M (2014) A review of zinc oxide mineral beneficiation using flotation method. Advances in Colloid and Interface Science 206:68-78. https://doi.org/https://doi.org/10.1016/j.cis.2013.02.003

[30]. Abkhoshk E, Jorjani E, Al-Harahsheh MS, Rashchi F, Naazeri M (2014) Review of the hydrometallurgical processing of non-sulfide zinc ores. Hydrometallurgy 149:153-167. https://doi.org/https://doi.org/10.1016/j.hydromet.2014.08.001

[31]. Li C, Wei C, Xu H-s, Li M, Li X, Deng Z, Fan G (2010) Oxidative pressure leaching of sphalerite concentrate with high indium and iron content in sulfuric acid medium. Hydrometallurgy 102:91-94. https://doi.org/https://doi.org/10.1016/j.hydromet.2010.01.009

[32]. Xu H, Wei C, Li C, Deng Z, Fan G, Li M, Li X (2014) Selective recovery of valuable metals from partial silicated sphalerite at elevated temperature with sulfuric acid solution. Journal of Industrial and Engineering Chemistry 20:1373-1381. https://doi.org/https://doi.org/10.1016/j.jiec.2013.07.021

[33]. Corriou J-P, Gély R, Viers P (1988) Thermodynamic and kinetic study of the pressure leaching of zinc sulfide in aqueous sulfuric acid. Hydrometallurgy 21:85-102. https://doi.org/https://doi.org/10.1016/0304-386X(88)90018-7

[34]. Costis S, Coudert L, Mueller KK, Cecchi E, Neculita CM, Blais J-F (2020) Assessment of the leaching potential of flotation tailings from rare earth mineral extraction in cold climates. Science of The Total Environment 732:139225. https://doi.org/https://doi.org/10.1016/j.scitotenv.2020.139225

[35]. Balaram V (2019) Rare earth elements: A review of applications, occurrence, exploration, analysis, recycling, and environmental impact. Geoscience Frontiers 10:1285-1303. https://doi.org/https://doi.org/10.1016/j.gsf.2018.12.005

[36]. Lie J, Liu J-C (2021) Selective recovery of rare earth elements (REEs) from spent NiMH batteries by two-stage acid leaching. Journal of Environmental Chemical Engineering 9:106084. https://doi.org/https://doi.org/10.1016/j.jece.2021.106084

[37]. Meshram P, Somani H, Pandey BD, Mankhand TR, Deveci H, Abhilash (2017) Two stage leaching process for selective metal extraction from spent nickel metal hydride batteries. Journal of Cleaner Production 157:322-332. https://doi.org/https://doi.org/10.1016/j.jclepro.2017.04.144

[38]. Maroufi S, Nekouei RK, Hossain R, Assefi M, Sahajwalla V (2018) Recovery of Rare Earth (i.e., La, Ce, Nd, and Pr) Oxides from End-of-Life Ni-MH Battery via Thermal Isolation. ACS Sustainable Chemistry & Engineering 6:11811-11818. https://doi.org/10.1021/acssuschemeng.8b02097

[39]. Kim J-Y, Shin C-H, Choi H, Bae W (2012) Recovery of phosphoric acid from mixed waste acids of semiconductor industry by diffusion dialysis and vacuum distillation. Separation and Purification Technology 90:64-68. https://doi.org/https://doi.org/10.1016/j.seppur.2012.02.013

[40]. Liu C, Deng Y, Chen J, Zou D, Su W (2017) Integrated Process To Recover NiMH Battery Anode Alloy with Selective Leaching and Multistage Extraction. Industrial & Engineering Chemistry Research 56:7551-7558. https://doi.org/10.1021/acs.iecr.7b01427

[41]. Wu S, Wang L, Zhao L, Zhang P, El-Shall H, Moudgil B, Huang X, Zhang L (2018) Recovery of rare earth elements from phosphate rock by hydrometallurgical processes – A critical review. Chemical Engineering Journal 335:774-800. https://doi.org/https://doi.org/10.1016/j.cej.2017.10.143

[42]. Schaeffer N, Passos H, Billard I, Papaiconomou N, Coutinho JAP (2018) Recovery of metals from waste electrical and electronic equipment (WEEE) using unconventional solvents based on ionic liquids. Critical Reviews in Environmental Science and Technology 48:859-922. https://doi.org/10.1080/10643389.2018.1477417

[43]. Quijada-Maldonado E, Romero J (2021) Solvent extraction of rare-earth elements with ionic liquids: Toward a selective and sustainable extraction of these valuable elements. Current Opinion in Green and Sustainable Chemistry 27:100428. https://doi.org/https://doi.org/10.1016/j.cogsc.2020.100428

[44]. Bertuol DA, Bernardes AM, Tenório JAS (2009) Spent NiMH batteries—The role of selective precipitation in the recovery of valuable metals. Journal of Power Sources 193:914-923. https://doi.org/https://doi.org/10.1016/j.jpowsour.2009.05.014

[45]. Marczenko Z, Balcerzak M (2000) Chapter 39 - Rare-earth elements. In: Marczenko Z, Balcerzak M (eds) Analytical Spectroscopy Library, vol 10. Elsevier, pp 341-349. https://doi.org/https://doi.org/10.1016/S0926-4345(00)80103-0

[46]. Ward FN, Nakagawa HM, Harms TF, Van Sickle GH (1969) Atomic-absorption methods of analysis useful in geochemical exploration. Bulletin, - edn. https://doi.org/10.3133/b1289
[47]. Shapiro L, Brannock WW (1962) Rapid analysis of silicate, carbonate, and phosphate rocks. Bulletin, - edn. https://doi.org/10.3133/b1144A
[48]. Kassab WA (2023) Comparative study for leaching processes of uranium, copper and cadmium from gibbsite ore material of Talet Seleim, Southwestern, Sinai, Egypt. Journal of Radioanalytical and Nuclear Chemistry 332:273-287. https://doi.org/10.1007/s10967-022-08727-x
[49]. Zheng X, Zhu Z, Lin X, Zhang Y, He Y, Cao H, Sun Z (2018) A Mini-Review on Metal Recycling from Spent Lithium Ion Batteries. Engineering 4:361-370. https://doi.org/https://doi.org/10.1016/j.eng.2018.05.018
[50]. Onghena B, Valgaeren S, Hoogerstraete TV, Binnemans KJRA (2017) Cobalt(II)/nickel(II) separation from sulfate media by solvent extraction with an undiluted quaternary phosphonium ionic liquid. 7:35992-35999
[51]. Chen W-S, Ho H-J (2018) Recovery of Valuable Metals from Lithium-Ion Batteries NMC Cathode Waste Materials by Hydrometallurgical Methods. Metals 8 (5). https://doi.org/10.3390/met8050321
[52]. Tuan LQ, Thenepalli T, Chilakala R, Vu HH, Ahn JW, Kim J (2019) Leaching Characteristics of Low Concentration Rare Earth Elements in Korean (Samcheok) CFBC Bottom Ash Samples. Sustainability 11 (9). https://doi.org/10.3390/su11092562
[53]. Zhou X, Chen Y, Yin J, Xia W, Yuan X, Xiang X (2018) Leaching kinetics of cobalt from the scraps of spent aerospace magnetic materials. Waste Management 76:663-670. https://doi.org/https://doi.org/10.1016/j.wasman.2018.03.051
[54]. Nayl AA, Elkhashab RA, Badawy SM, El-Khateeb MA (2017) Acid leaching of mixed spent Li-ion batteries. Arabian Journal of Chemistry 10:S3632-S3639. https://doi.org/https://doi.org/10.1016/j.arabjc.2014.04.001
[55]. Cao Z-f, Zhong H, Liu G-y, Zhao S-j (2009) Techniques of copper recovery from Mexican copper oxide ore. Mining Science and Technology (China) 19:45-48. https://doi.org/https://doi.org/10.1016/S1674-5264(09)60009-0
[56]. Clotilde Apua M, Madiba MS (2021) Leaching kinetics and predictive models for elements extraction from copper oxide ore in sulphuric acid. Journal of the Taiwan Institute of Chemical Engineers 121:313-320. https://doi.org/https://doi.org/10.1016/j.jtice.2021.04.005
[57]. Su H, Liu H, Wang F, LÜ X, Wen Y (2010) Kinetics of Reductive Leaching of Low-grade Pyrolusite with Molasses Alcohol Wastewater in H2SO4. Chinese Journal of Chemical Engineering 18:730-735. https://doi.org/https://doi.org/10.1016/S1004-9541(09)60121-X
[58]. Kim C-J, Yoon H-S, Chung KW, Lee J-Y, Kim S-D, Shin SM, Lee S-J, Joe AR, Lee S-I, Yoo S-J, Kim S-H (2014) Leaching kinetics of lanthanum in sulfuric acid from rare earth element (REE) slag. Hydrometallurgy 146:133-137. https://doi.org/https://doi.org/10.1016/j.hydromet.2014.04.003
[59]. Dickinson CF, Heal GR (1999) Solid–liquid diffusion controlled rate equations. Thermochimica Acta 340-341:89-103. https://doi.org/https://doi.org/10.1016/S0040-6031(99)00256-7
[60]. Salem AR, Kassab WA (2020) Uranium and rare earth elements leaching characteristics from El-Sella mineralized Granite, Eastern Desert, Egypt. International Journal of Environmental Analytical Chemistry:1-25. https://doi.org/10.1080/03067319.2020.1832479
[61]. Liu ZX, Yin ZL, Xiong SF, Chen YG, Chen QY (2014) Leaching and kinetic modeling of calcareous bornite in ammonia ammonium sulfate solution with sodium persulfate. Hydrometallurgy 144-145:86-90. https://doi.org/https://doi.org/10.1016/j.hydromet.2014.01.011
[62]. Prameswara G, Trisnawati I, Poernomo H, Mulyono P, Prasetya A, Petrus HTBM (2020) Kinetics of Yttrium Dissolution from Alkaline Fusion on Zircon Tailings. Mining, Metallurgy & Exploration 37:1297-1305. https://doi.org/10.1007/s42461-020-00220-x
[63]. Wang L, Chen M, Li J, Jin Y, Zhang Y, Wang Y (2020) A novel substitution-based method for effective leaching of chromium (III) from chromium-tanned leather waste: The thermodynamics, kinetics and mechanism studies. Waste Management 103:276-284. https://doi.org/https://doi.org/10.1016/j.wasman.2019.12.039
[64]. Eshuis A, van Elderen GRA, Koning CAJ (1999) A descriptive model for the homogeneous precipitation of zinc sulfide from acidic zinc salt solutions. Colloids and Surfaces A: Physicochemical and Engineering Aspects 151:505-512. https://doi.org/https://doi.org/10.1016/S0927-7757(98)00835-8
[65]. Veeken AHM, Akoto L, Hulshoff Pol LW, Weijma J (2003) Control of the sulfide (S2−) concentration for optimal zinc removal by sulfide precipitation in a continuously stirred tank reactor. Water Research 37:3709-3717. https://doi.org/https://doi.org/10.1016/S0043-1354(03)00262-8
[66]. Esposito G, Veeken A, Weijma J, Lens PNL (2006) Use of biogenic sulfide for ZnS precipitation. Separation and Purification Technology 51:31-39. https://doi.org/https://doi.org/10.1016/j.seppur.2005.12.021
[67]. Habashi F (2000) A Textbook of Hydrometallurgy, 2nd edition. Fathi Habashi 13. https://doi.org/10.1016/S0892-6875(00)00127-8
[68]. Mubarok MZ, Lieberto J (2013) Precipitation of Nickel Hydroxide from Simulated and Atmospheric-leach Solution of Nickel Laterite Ore. Procedia Earth and Planetary Science 6:457-464. https://doi.org/https://doi.org/10.1016/j.proeps.2013.01.060
[69]. Eliwa AA, Gawad EA, Mubark AE, Abdelfattah NA (2021) Intensive Studies for Modeling and Thermodynamics of Fusion Digestion Processes of Abu Rusheid Mylonite Rocks. JOM 73:3419-3429. https://doi.org/10.1007/s11837-021-04837-1
[70]. Gawad EA (2020) A Novel Technique: Conceived Predictive Diagonal (CPD) Graphical Nonlinear Regression Modeling and Simulation.213-220